



Philipp Sulzer, BSc

Utilization of microdispensing technology for the application of optical sensors

MASTER THESIS

for the aquisition of the academic title

Master of Science (MSc)

Master Program "Technical Chemistry"

submitted at

University of Technology Graz

Supervisor:

Assoc. Prof. Dr. Torsten Mayr

Institute for Analytical Chemistry and Food Chemistry

Graz, April, 2016

Abstract

The goal of this thesis was the evaluation of microdispensing technology as an application method for optical sensors. After attachment of the microdispenser to a CNC machine and software development for the control an elaborate search for fitting sensor formulation compositions as well as spotting parameters was executed. By varying polymer viscosities, solvents and solvent mixtures, nozzle distance, droplet exit speed and other parameters, a solid dispensing methodology was found to print sensor spots down to 250 μm diameter as well as larger sensor layers with relatively flat surfaces and adjustable layer heights.

After finding sufficient compositions for dissolved oxygen sensors, a procedure had to be found to disperse larger ceramic particles (up to 30 μm) for the pH sensor. Therefore, an ultrasonic dispersion process has been employed as well as increased cocktail viscosity to diminish precipitation effects throughout the printing process.

Evaluation and analysis of more than 500 produced sensors showed satisfying reproducibility regarding oxygen sensors and potential for improvement regarding pH, since precipitation effects could not be eliminated fully. However, it was shown that sensor production of at least 150 working sensor spots in a single batch is possible without significant interferences like clogging.

As a result of this thesis an easy-to-use sensor printer for oxygen and pH sensor spots and layers was developed including easily usable software. The device may also be used for other sensor applications with different solvents, matrices and dyes.

Kurzfassung

Das Ziel dieser Masterarbeit war die Entwicklung und Analyse eines Druckgeräts zur Aufbringung für optische Sensoren auf Basis eines Mikrodosiergerätes. Nach Anschluss an ein CNC System und Entwicklung von Software für Positionierung und Druckkopf wurde der größte Teil der Arbeit darauf konzentriert, passende Sensor-Cocktail Zusammensetzungen sowie Druckparameter zu finden. Durch ausgedehnte Tests mit verschiedenen Lösungsmitteln, Polymerlösungsviskositäten, Düsenabständen, Tropfenaustrittsgeschwindigkeiten und anderen Parametern konnte schlussendlich eine brauchbare Umgebung zum Sensordruck geschaffen werden. Zum momentanen Zeitpunkt können Sensorspots ab 250 μm sowie größere Sensorschichten mit relativ flachen Oberflächen und einstellbarer Schichtdicke produziert werden.

Zusätzlich zur Verwendung für gelöste Sensorcocktails wie der verwendete O_2 Sensor musste für pH auch eine Möglichkeit gefunden werden, größere Keramikpartikel (DLR Referenzpartikel bis 30 μm) für längere Zeit in einer möglichst stabilen Dispersion zu halten. Hierzu wurde die Polymerlösungsviskosität erhöht, sowie Ultraschalldispersion verwendet, um Partikelniederschlag während des Druckens möglichst zu vermeiden.

Nach der Produktion und Kalibration von über 500 Sensoren konnte eine zufriedenstellende Reproduzierbarkeit für O_2 und diesbezügliches Verbesserungspotenzial für pH festgestellt werden. Die Niederschlagsgeschwindigkeit der Referenzpartikel für den DLR pH Sensor war zwar hoch genug, um das Kalibrationsverhältnis über fortschreitende Produktion zu verändern, allerdings konnten 150 funktionierende Sensoren in einem Anlauf produziert werden.

Als Ergebnis dieser Arbeit konnte ein verwendbares Drucksystem für Sauerstoff und pH Sensoren inklusive einfach handhabbarer Software entwickelt werden. Basierend auf dieser Arbeit besteht eine Basis für zukünftige Anwendungen anderer Sensoren wie Glucose, CO_2 , NH_3 und andere.

EIDESSTATTLICHE ERKLÄRUNG

Ich erkläre an Eides statt, dass ich die vorliegende Arbeit selbstständig verfasst, andere als die angegebenen Quellen/Hilfsmittel nicht benutzt, und die den benutzten Quellen wörtlich und inhaltlich entnommenen Stellen als solche kenntlich gemacht habe. Das in TUGRAZonline hochgeladene Textdokument ist mit der vorliegenden Masterarbeit identisch.

Datum/Date

Unterschrift/Signature

Acknowledgement

Als ich sechs Jahre alt war, wollte ich Baggerfahrer werden. Mit acht Jahren hatte ich den Traum, eines Tages Jetpilot zu werden. Seit meinem zwölften Lebensjahr ungefähr wollte ich jedoch Wissenschaftler werden. So ein Typ im Labormantel, der Sachen zusammenleert. Und bastelt. Und mit Computern spielt. So habe ich mir meine zukünftige Arbeit die letzten fünfzehn Jahre vorgestellt. Diese Diplomarbeit ist ein Resultat siebenmonatiger Arbeit, die ziemlich genau so war, wie ich es mir mit zwölf schon gewünscht hätte. Dass es dazu kommen konnte, verdanke ich einer ganzen Menge Personen, die ich nun nennen möchte.

An erster Stelle möchte ich meiner Mutter danken. Jener Person, die mir immer alles ermöglicht hatte, obwohl viele meiner Interessen nicht länger als zwei Monate andauerten. Die kaum benutzten Golfschläger und der gelbe Tae-Kwon-Do Gürtel sprechen für sich. Dass ich nach Wels gehen konnte und meine Zeit in Graz immer sorgenfrei war verdanke ich dir. Dass ich noch immer gerne nach Hause komme, verdanke ich aber natürlich auch anderen. Zum Beispiel Sandra und Stefan, meinen beiden freshen Lieblingsgeschwistern, die sehr oft mit mir und manchmal über mich lachen, weil ich Jugendslang benutze, der so nicht existiert. Auch meiner lieben Oma möchte ich natürlich danken, von der ich nur Zuspruch, Unterstützung und Fürsorge erfahren habe. Und wenn wir schon beim zweiten Zuhause sind, möchte ich Tante Maria, Onkel Mike und Sarah und Thomas natürlich nicht vergessen. An dieser Stelle ist es mir noch wichtig, einen speziellen Gruß an Erwin zu richten, dem ich wahrscheinlich mehr verdanke, als er sich denken kann.

Meine chemische Karriere begann in der HTL Wels und wurde geprägt von Prof. Sagmüller und Prof. Eibl. Auch wenn sich nicht immer alles um Moleküle und Enthalpien drehte. Manchmal gings einfach um Bier, laute Musik und gute Freunde. Gute Freunde wie Mike, Jack, Alex, Corni, Ewald und der Rest der Stammtischgang. In Graz kamen dann viele neue Leute dazu. Jene heißen Sepp, Georg, Rene, Nici oder Melanie zum Beispiel. Die sind nur ein Teil einer sehr elitären Gruppe, die sich selbst „Die Dumpfbacken“ nennt und mitunter ein Hauptgrund für meine Liebe für Graz ist. Besonders wichtig erscheint es mir allerdings, hier noch Fex und Luki zu erwähnen, die meine letzten sechs Jahre hier besonders geprägt haben.

Dass ich auf dem besten Institut der Welt arbeiten durfte, tat meiner Freude natürlich auch keinen Abbruch. Mit Heidi, Silvia und Berni hatte ich die besten Bürokollegen, die man sich nur wünschen kann. Die Alte Garde (eingesessene PhDs), die New Generation und der Rest der ACFC Bande machen diesen Arbeitsplatz zu etwas Besonderem. Und natürlich ein fettes Danke an Tobi, Eveline und Ingo, die mir ermöglicht haben, hier als Oompa Loompa anzuheuern.

Mit Josef und Birgit sind hier noch zwei sehr wichtige Personen aufzulisten. Von euch habe ich sowohl menschlich, als auch fachlich unglaublich viel mitgenommen. Ich war mir immer bewusst, welches Glück ich hatte, euch als Betreuer zu haben. Genauso steht es mit Torsten. Für das Vertrauen, das du mir seit mehr als drei Jahren entgegenbringst, möchte ich mich bedanken.

Den letzte Dank möchte ich noch Anna ausstellen. Die letzten zweieinhalb Jahre waren eine schöne Reise, die ohne dich nicht halb so schön gewesen wäre.

Contents

1	Introduction	1
2	Theoretical Background	2
2.1	Application methods for polymer layers	2
2.1.1	Knife coating	2
2.1.2	Spraying	3
2.1.3	Spin coating	4
2.1.4	Screen printing	4
2.1.5	Inkjet printing	5
2.1.6	Aerosol jet printing	6
2.2	CNC - computerized numerical control	7
2.2.1	Working principle of CNC	8
2.3	Optical sensors	8
2.3.1	Luminescence background	8
2.3.2	Luminescence lifetimes and quenching	9
2.3.3	Frequency domain luminescence lifetime measurement	12
2.3.4	Single fiber luminescence measurement	13
2.3.5	Dual lifetime referencing - DLR	13
3	Experimental	16
3.1	Materials and equipment	16
3.1.1	Devices	16
3.1.2	Substances	17
3.2	Three axis movement by computerized numerical control (CNC)	18
3.3	Installation of the microdispensing system	18
3.4	Provision of a setup interface for microdispensing	20
3.4.1	Movement and triggering - LinuxCNC	20
3.4.2	Dispensing parameters - LabView	22
3.5	Preparation of polymer layers and spots by microdispensing	23
3.6	Determination of the influence of different parameters on spot appearance	26
3.7	Reference particle dispersing	27
3.8	Evaluation of dispensing reproducibility	28
3.8.1	Preparation of multiple sensor spots and layers on PMMA slides	28
3.8.2	Automated evaluation readout system	29
3.9	Preparation of multilayer pH sensors	30
3.10	Preparation of intermediate layers for dye migration prevention	31
3.10.1	Preparation of intermediate layers with varying thicknesses	32
3.10.2	Sensor printing on intermediate layers	32

4	Results and Discussion	34
4.1	Determination of the influence of different parameters on spot appearance . . .	34
4.1.1	Tappet lift	34
4.1.2	Falling time	36
4.1.3	Pressure	38
4.1.4	Distance	39
4.2	Egyptian Blue dispersing	40
4.3	Reproducibility evaluation of single spot and layer sensors	42
4.3.1	Reproducibility evaluation of oxygen sensors	42
4.3.2	Reproducibility evaluation of pH sensors	47
4.4	Multilayer pH sensors	51
4.5	Influence of spot distance on layer profile	52
4.6	Evaluation of dye migration prevention through PS intermediate layers	55
5	Conclusion and Outlook	57
6	References	60
7	List of Figures	63
8	List of Tables	65
9	Appendix	67
9.1	CNC control (G-code)	67
9.2	Profile measurement file conversion (python)	68

1 Introduction

Optical sensors represent a powerful tool for specific analytical measurements due to a few characteristics compared to conventional analytical tools:

- utilization of optical effects such as absorption and luminescence
- no direct intrusion with electric current
- possibility of measurements in closed systems from outside
- multiple analyte readouts on a single device through interchangeable sensors
- no reference elements
- contact-less measurement

Optical sensors have been prepared for the detection of pH [1], O₂ [2], NH₃ [3], glucose [4] and Cu²⁺ [5] for example. Optical sensors can be applied on fibers for direct contact measurements as probes (optodes or optrodes), implemented on surfaces or inside closed systems such as transparent reaction vessels or microfluidic devices. Application methods for optical sensors are printing and coating techniques such as knife or spin coating.

Within the work of this thesis, a rather recent approach on a wide variety of sensor application needs was taken. A sensor printer for different applications was developed by utilization of a microdispenser. The goal was to be able to produce small sensors at sizes below 1 mm as well as larger sensor layers up to 1 cm. Ultimately the device should be able to apply sensors to mid scale macrofluidic devices (>250 μm channel width), flat glass and polymer substrates as well as foils, microtiterplates, macrofluidic batch devices and similar applications.

Since the device is meant to be used as a multifunctional sensor printer, microdispensing was the technology of choice. It combines advantages of inkjet systems such as motive customization and printing speed with a significantly increased variety of solvent and viscosity range as well as fast medium exchange.

A major part of the work besides the physical installment was dedicated to finding suitable parameters regarding printing setup and sensor formula composition. At the end of this thesis a sensor printer is provided including state-of-the-art procedures for printing oxygen and pH sensors.

2 Theoretical Background

2.1 Application methods for polymer layers

Printing layers of polymers on different substrates is a rather extensive field. There is no technology that can be awarded as the best application method for polymer layers. The technique that is used depends on different factors as:

- size of the desired printed area
- printing resolution
- polymer solution composition (solvent, viscosity,...)
- layer thickness
- printing time
- direct contact or contactless printing
- substrate surface (roughness, flat or structured)
- necessity of motive change

2.1.1 Knife coating

Of all the presented layer application method knife coating is the fastest method. Similar to screen printing, the often viscous solution is applied onto a flat substrate and then spread along.

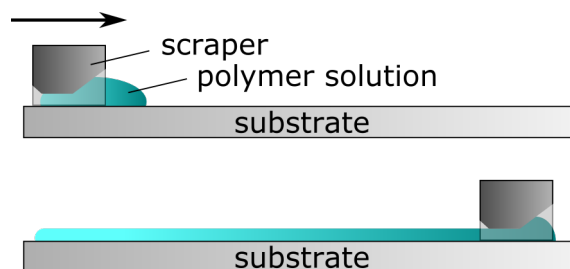


Figure 2.1: Schematic presentation of a knife coating process

Knife or blade coating can be executed with or without printing mask. Without mask the surface is covered by the width and height of the blade and the desired length. With mask, the process is very similar to screen printing, where only the specific motives are applied. The method is very suitable for fast coating of large areas if used without a mask. A research field that is interested in this technology is the production of organic photovoltaic cells [6]. It is also possible to cover strips of layers over the edges by using different knife widths. Knife coating

can also be an interesting technology for the production of functional materials. Trommer et. al. showed a method to create electrically conductive PVC layers with heights of 100 μm and below [7]. Using masks, it is also capable of fast and reliable manufacturing of structured multilayer components such as flexible organic transistors on polymer foils [8]. Due to its affordability and the ability of fast prototype layer production knife coating is the method of choice for quick laboratory tests and research that do not necessarily demand structured motives or completely homogenous flat layers. This way, optical sensors have been prepared by knife coating for analytes such as ammonia [9] and pH [10] for example.

Besides the advantages the method shares with screen printing, it also faces similar restrictions. The substrate has to be flat and is not allowed to have a structured surface. Really small structures are difficult to realize by masks. Another way to create structured knife coated layers is by post processing such as cutting. Here the removal of the layer from the substrate and its reapplication to another surface takes a lot of effort.

2.1.2 Spraying

Usually carried out with an airbrush system, spray coating needs a (compared to other printing methods) relatively low viscosity regarding the desired solution. The cocktail is guided through a small conduit that can be closed and continuously opened by a needle. Surrounding the spray nozzle is the pressure outlet. The enclosing stream of air or inert gas leads to a fine dispersal and a stream of fine cocktail drops.

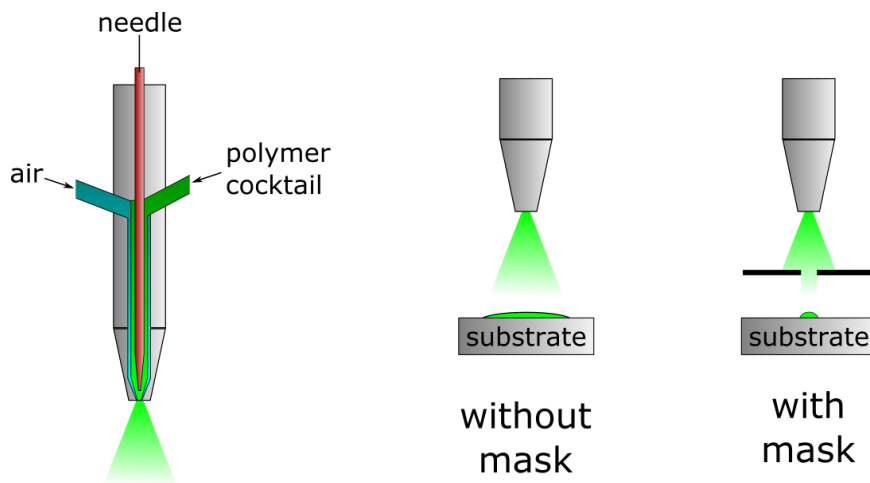


Figure 2.2: Working principle of spray coating with and without mask

Due to the conical nature of the spray beam creating very small structures would be a challenge without additional aid. Therefore, masks can be used to apply structures or motives. This way oxygen sensor spots have already been prepared with sizes down to 100 μm [11]. Similarly to knife coating and screen printing the ability of covering large areas with considerable homogeneity is an interesting aspect for the production of solar cell and battery compounds. Kumar et al. showed the applicability of spray coating for the preparation of active layers for photovoltaic systems [12]. Regarding the development of lithium ion batteries, cathodes [13] and separators [14] have already been realized through spraying. Further it has also been used for the coating of electronic structures with thin polymer films during through silicon production [15].

Compared to inkjet printing spraying would rather be chosen if larger areas have to be covered. Creating predetermined motives demands additional effort in mask preparation. Also, using spraying masks can lead to significant loss of cocktail material and regaining dried residue might be a challenge. A further restriction with spraying is that the spray beam does not have a consistent spray intensity. The center of the jet transports more cocktail than on the radial outside. This has to be considered when flat surfaces with narrow roughnesses are demanded.

2.1.3 Spin coating

Spin coating is an application technology that can produce polymer layers with relatively low layer thicknesses (compared to other mentioned methods) and rather flat surfaces. The polymer formula, ink or particle dispersion is applied to the center of a rapidly spinning substrate. The liquid or gel is distributed throughout the surface due to centrifugal force.

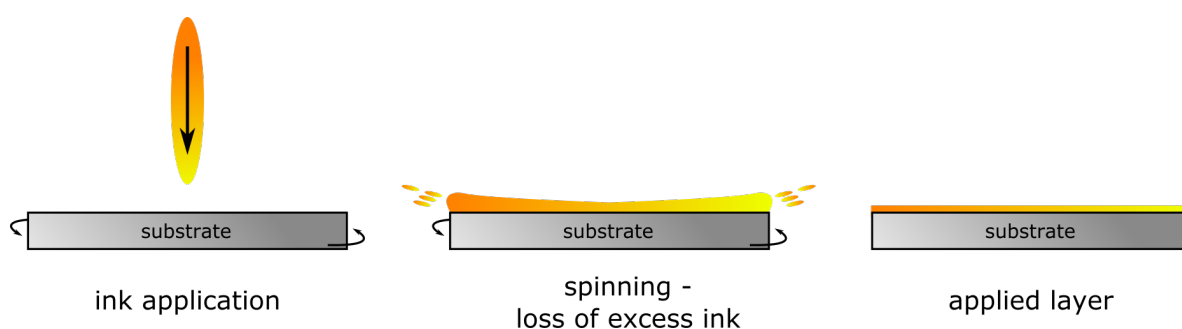


Figure 2.3: Layer application through spin coating

Spin coating is often used as the method of choice for organic photovoltaics production due to its potential for homogenous layer formation and the possibility of multiple layer application. For OPVs basically every layer besides the metal electrode can be applied by spin coating [16]. The method can also be used for the production of ultra thin semiconducting films with layer thicknesses below 10 nm [17]. By using sol-gel spin coating it is also possible to grow nanocrystalline structures on the substrate. This technique was used to produce SnO_2 thin film hydrogen gas sensors for example [18]. Optical sensors have also been successfully prepared by spin coating, shown in [19] for pH and [20] for oxygen.

The method is very reproducible and fast, but either leads to high material loss of excess ink or demands a rather complicated recycling mechanism. It is best suitable for flat substrates without structures and usually covers the the whole surface. Motive printing demands application masks that can add further complications to the whole process.

2.1.4 Screen printing

Screen printing is a very common method for material application when it comes to high repetition counts. A specially prepared mesh is applied to the substrate and the polymer cocktail is distributed over the whole motive through spreading.

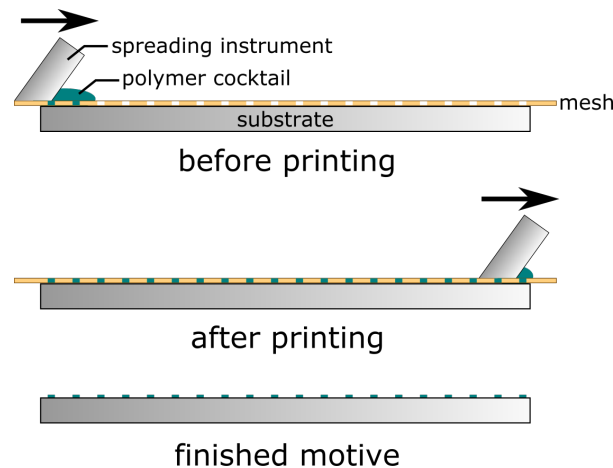


Figure 2.4: Schematic presentation of a screen printing process

The main characteristic of screen printing is its ability of very high repetition cycles. Since there is no printing head that has to move onto every single structure element (pixel i.e.), the motive is created very fast through spreading of the cocktail over the mesh. This advantage is very interesting for production fields, where large flat areas have to be printed in short time. The method is especially useful in recent research topics as organic photovoltaics. Krebs et al. produced solar cells where every single layer beginning with silver electrodes, PEDOT and P3CT, ZnO and ITO were screen printed one after another [21]. Besides this use for large surface areas screen printing can also be used for relatively small structures such as electrodes for electrochemical sensors in microfluidics [22]. With appropriate mesh and ink composition structures down to 35 μm can be achieved. In context to this thesis also optical sensors shall be mentioned. Mayr et al. showed screen printed opto-electronic sensors for oxygen, carbon dioxide, ammonia and temperature [23].

With all the advantages of screen printing there are physical restrictions as well. Fast motive individualization is not given due to the necessity of mesh preparation. Also, the mechanism enforces use of completely flat substrates, making the method unsuitable for three dimensionally structured substrates such as microfluidic channels or microtiterplates. The relatively high material waste generation compared to other printing methods is also a disadvantage.

2.1.5 Inkjet printing

Inkjet printing is a very established medium application technology ranging from consumer use, industrial large scale printing and various research and development fields. Contrary to screen printing, inkjet systems dispense small drops of solutions or dispersions one by one either by mechanical force or thermal energy impact [24].

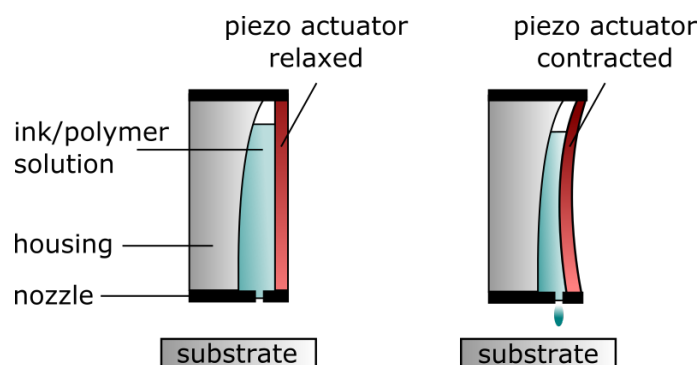


Figure 2.5: Droplet ejection through mechanical piezo contraction

Through specific design of nozzle, housing and dispensing mechanism very small structure sizes can be achieved down to $15\ \mu\text{m}$ [25]. The possibility of high resolution compared with free two-dimensional placement freedom awards inkjet printing very often as method of choice for tasks where high individualization and/or contactless application are demanded. There are two main working principles how inkjet printing can be realized. Continuous inkjet printers generate a continuous stream of drops that are electromagnetically deflected either onto the substrate or into a recycling gutter [26]. This technology is applied in industrial uses due to its high printing speed. For smaller applications drop-on-demand (DOD) systems are used. A piezoelectric ejection head (Figure 2.5) for example only produces droplets when it is electrically triggered. The same principle applies for thermal DOD printers, where the exit energy is produced by water vapor bubbles heated up to 450°C .

Besides the broad use in colour printing industry there has been high interest in inkjet systems for research and development use. It is especially useful in sensor preparation such as surface enhanced Raman spectroscopy (SERS) microsensors [27] or biosensors for oxygen peroxide measurements [28]. A recent research field where inkjet printing can be applied is sensor integration for microfluidic systems. In-channel sensors have been already realized for monitoring flow rates [29] and pH [30] for example.

The relatively low speed compared to screen printing has no influence in the relevance of inkjet regarding small structures such as sensor production for research purposes. The more important restrictions however lay in the very narrow range considering ink viscosity, choice of solvent and particle size.

2.1.6 Aerosol jet printing

Aerosol jet printing is a relatively new technology for layer and particle application. Produced structures can be as small as $20\ \mu\text{m}$ [31]. The mechanism is based on initial aerosol formation through carrier gas flow into a specially designed reservoir chamber. The aerosol is then led through a so called impactor, where excess gas is let out and the printing aerosol is further transported to the nozzle. Here a small beam of finely dispersed ink droplets are sprayed onto the substrate surface.

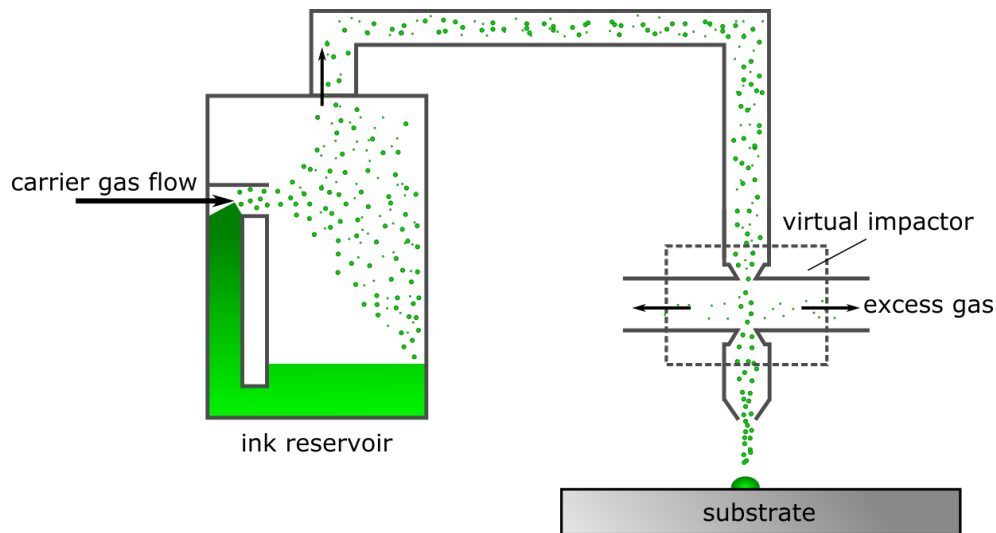


Figure 2.6: Layer application by aerosol jet printing

The technology is particularly suitable for application in electronics and is widely used for fast preparation of custom printed integrated circuits. In [32] a printing method is shown for highly flexible conductive graphene/silver layers with structure sizes below $50\ \mu\text{m}$. In addition to the conductive components aerosol jet printing has also been used to prepare electronic elements such as OLEDs [33] and thin film transistors [34].

High resolution and a wide spectra of printable materials are some of the main advantages of aerosol jet printing. With the necessity of low viscosity inks and inability of printing large particles the method has rather similar restrictions as inkjet printing.

2.2 CNC - computerized numerical control

Fundamental information for this chapter was taken out of [35] and [36].

So called computerized numerical control systems state the most important part of automated flexible production systems besides integrated robotics. These so called "digital manufacturing" methods are used for their adaptability regarding different workpieces, the wide material and dimension range as well as their broad arsenal of tool collections. The industry appreciates CNC technology not only for the uncomplicated customizability and precision. What is also highly valued is its use as a one-in-all hybrid manufacturing tool. One or more of the following machining techniques can be integrated in CNC devices:

- mill turning
- grinding
- laser cutting
- milling

Further, those systems can also be used for positioning purposes like sampling, measurement tasks, placement or sorting. In this thesis, CNC has been used for sensor printing and subsequent calibration. This utilization for applications other than usual workpiece machining also shows the broad range of individualization for computerized numerical control.

2.2.1 Working principle of CNC

Tool machines rely on positioning and timing for operation. Before integration of numerical control this process was controlled either by human operation or the use of moving templates and cam discs. This caused poor adaptability and demanded a lot of time and resources regarding customization. Also adjustment and calibration was a time consuming process, increasing exponentially with desired accuracy. With the integration of numerical control a lot of those disadvantages could be countered. NC systems are designed to "translate" numbers into movement. Information for position, movement speed, tool management and triggering for binary elements (valves, grips,...) are transferred electronically. The NC system then follows the orders in real time. What became necessary was the ability for high resolution positioning and calibration as well as electrical adjustability. The first numerical control systems used relays and did not automatically have better adjustability, since the electric circuits were static and there was no way of programming.

By adding computers (thus, **computerized** numerical control), manufacturing became significantly more versatile. CNC programs can be written and changed almost at will, the only restrictions being computing resources and physical limits of the executing machinery. CNC machines are controlled either by standalone processing computers or specially equipped personal computers (see 3.2). Mainstream operating systems for large audiences are not well-suited for CNC applications due to the high amount of background processes running. Real time machinery programming is very delicate and can even lead to physical damage and injury if handled incautiously.

Programming a CNC system works on three different levels. The **operating system** basically controls computing, input and output. The **machine specific software** provides detailed information on the physical system like calibration, step resolution and movement interpretation. On the surface, the **standard software** works as an input instrument for the user. On this level, data (3D models i.e.) is entered and may be reviewed or even changed before the process is started.

2.3 Optical sensors

Most of the information regarding this chapter was gathered by the two textbooks [37] and [38].

Optical sensors can be a powerful alternative to common traditional analytical methods. Advantages of optical sensors are their ability for contact-less measurement, multi-analyte analysis and the functionality without direct reference systems. There are already existing optical sensor technologies for a range of analytes. In this thesis, oxygen and pH sensors are used. Although the measurement system for both analytes is the same, the fundamental principles are different. The following sections should pose a short overview on said working principles.

2.3.1 Luminescence background

There are basically two initial scenarios that can happen when radiation meets matter. Transmission means no interaction of the radiation with the material at all. So called transparent materials have a high amount of transmittance and therefore let large parts of the discussed irradiation through. Absorption on the other hand is what happens when radiation and matter actually interact. It leads to excitation and is only an initial step for a row of physical steps

that can happen afterwards.

For optical sensors there are different working principals like absorption, luminescence intensity and lifetime or electro-optical sensors that convert radiation to electric signals. For this thesis, VIS-NIR (visible light - near infrared) luminescence based sensors were used. Luminescence happens after excitation and leads to emission of usually lower energy rays (unless upconversion is happening) after some time.

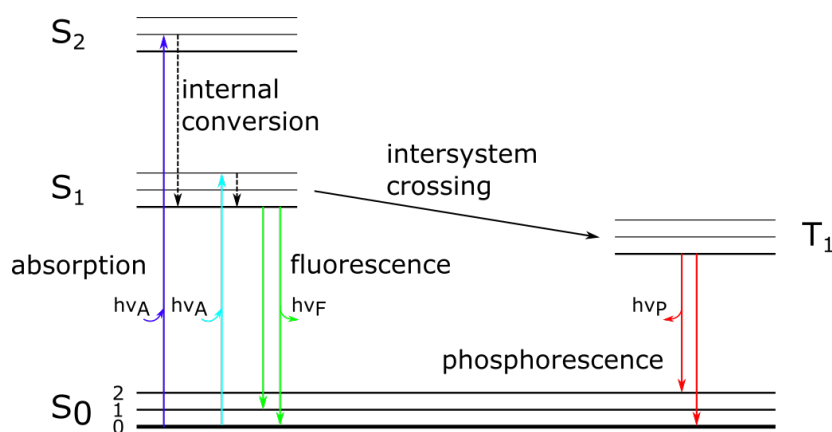


Figure 2.7: Jablonski diagram

Figure 2.7 shows the so called Jablonski diagram. It demonstrates the electronic excitation of an irradiated molecule from ground state (S_0) to the first and second electronic states S_1 and S_2 and their respective vibrational energy levels (depicted as thin energy levels 1 and 2). Internal conversion leads to electronic relaxation back to the lowest vibrational level of S_1 in most cases observable. This process happens within a time span of 10^{-12} s or less. After this pre-relaxation there are different ways of the electronic energy to develop. If the direct relaxation to S_0 emits light the emission is called fluorescence. The time scale of this process is about 10^{-8} s. Fluorescence relaxation does not typically occur to different vibrational states of S_0 , leading to non-defined emission spectra. On the other hand, if (quantum mechanically actually forbidden) spin conversion from singlet to triplet occurs, the transition is called intersystem crossing. Any further development from the T_1 state to either S_1 (further relaxation and emission is then called delayed fluorescence) or directly to S_0 (the so called phosphorescence) is also forbidden due to the spin conversion. Any emission, that undergoes intersystem crossing is significantly slower than fluorescence. There is also the possibility for radiation less relaxation back to S_0 . The rates of emissive and nonradiative decay are used to determine the quantum yield of a luminescence system (see 2.3.2) Contrary to Raman emission, the nature of luminescence physics leads to distinct spectra in spite of different excitation energies.

2.3.2 Luminescence lifetimes and quenching

Luminescence lifetime describes the timespan in which the emission happens. Whereas fluorescence lifetimes are usually within nanosecond scale, phosphorescence lifetimes tend to be magnitudes longer, depending on the nature of the molecule and its surroundings. A crucial part that affects the lifetime are the rate constants for luminophore emission (Γ) and non-radiative decay to S_0 (k_{nr}). The quantum yield Q of a luminophore system is calculated from those

constants:

$$Q = \frac{\Gamma}{\Gamma + k_{nr}} \quad (2.1)$$

Q	...	quantum yield
Γ	...	emissive rate of fluorophore
k_{nr}	...	rate of nonradiative decay to S_0

The luminescence lifetime τ is a result of a combination of both radiative and non-radiative relaxation processes. It is given as:

$$\tau = \frac{1}{\Gamma + k_{nr}} \quad (2.2)$$

τ	...	luminescence lifetime
--------	-----	-----------------------

The quantum yield Q is important for the luminescence intensity. High Q values lead to stronger emission intensities and are usually desired in optical sensor research and application. Lifetimes on the other hand are connected to a lot of different physical and chemical parameters such as molecular structure, temperature, surrounding matrix and possible quenchers. Luminescence quenching describes the reduction of emission intensity and/or lifetime by interaction of the luminophore with surrounding molecules. There are different mechanisms of quenching:

Static quenching

Static quenching does not affect the luminescence lifetime. The mechanism behind static quenching relies on the formation of a quencher-luminophore complex (QL).

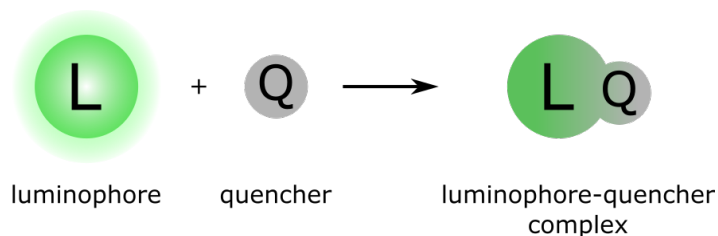


Figure 2.8: Luminescence quenching through complex formation

For optical sensors, this mechanism can be used for analyte concentration measurements through intensity observation. Here the analyte is also the quenching molecule that further decreases luminescence intensity at higher concentrations.

Dynamic quenching

Contrary to its static counterpart dynamic quenching not only leads to reduced luminescence intensity but also lowers the lifetime at higher quencher concentrations.

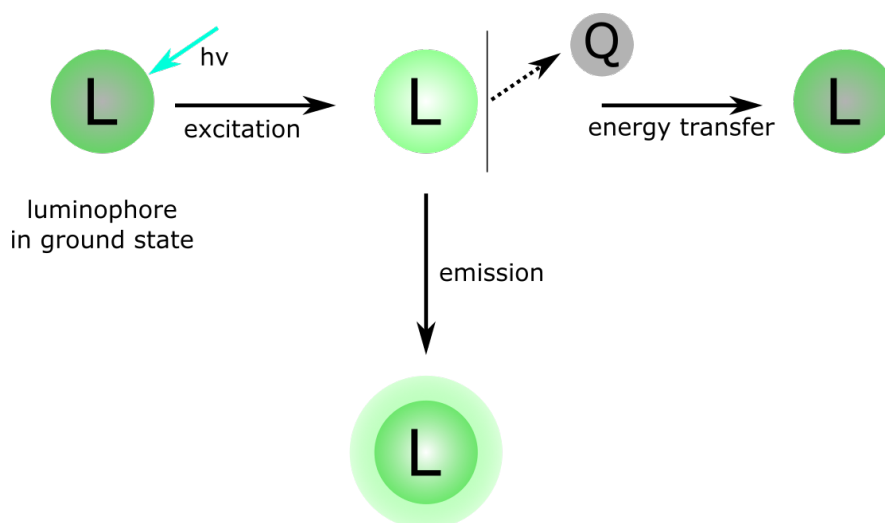


Figure 2.9: Dynamic quenching mechanism

This mechanism demands the luminophore and the quenching molecule to collide for energy transfer, therefore the term "collisional quenching" can also be used. The lifetime and intensity decrease at higher quencher concentrations is given as the Stern-Volmer equation:

$$\frac{I_0}{I} = \frac{\tau_0}{\tau} = 1 + k_Q \tau_0 [Q] = 1 + K_{SV} [Q] \quad (2.3)$$

I_0	...	luminescence intensity in absence of quencher
I	...	luminescence intensity at given quencher concentration
τ_0	...	luminescence lifetime in absence of quencher
τ	...	luminescence lifetime at given quencher concentration
k_Q	...	bimolecular quenching constant
$[Q]$...	quencher concentration
K_{SV}	...	Stern-Volmer constant

Photoinduced Electron Transfer - PET

Similar to static quenching, photoinduced electron transfer also relies on the formation of a complex. The terminology in this case however uses donor and acceptor for the involved molecules, since a redox reaction is occurring.

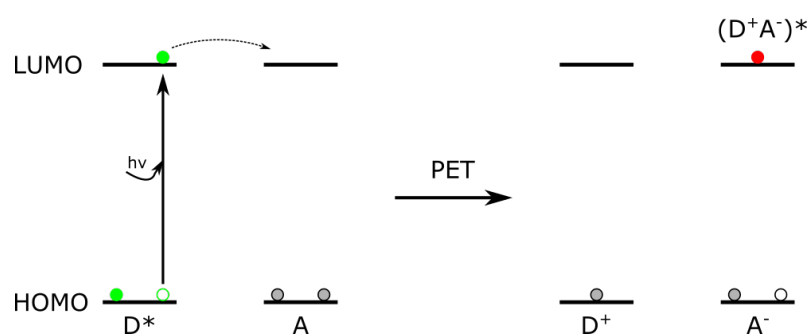


Figure 2.10: Photoinduced electron transfer

For PET systems the luminophore can be either donor or acceptor. In Figure 2.10 the luminophore is shown as electron donor. After excitation, the electron is transferred to the acceptor, leaving a complex with oxidized luminophore and reduced quencher. This so called charge transfer complex can return to the respective ground state without light emission, therefore prohibiting the luminescence. PET can occur inter- or intramolecularly. The pH indicating dye used in this thesis (see 3.1.2) contains donor and acceptor covalently bonded and depends on the protonation and deprotonation of the molecule for switching the PET effect on and off [39].

2.3.3 Frequency domain luminescence lifetime measurement

To use luminescence molecules as sensors, emission intensity and/or lifetime has to be measured. Analysis of optical sensors within this thesis was done by phase fluorimetry. For this method, the sensor is illuminated by a sinusoidal excitation signal. Due to the nature of a luminophore to stay excited for some time before relaxation (lifetime τ), the emission signal is delayed (see Figure 2.11).

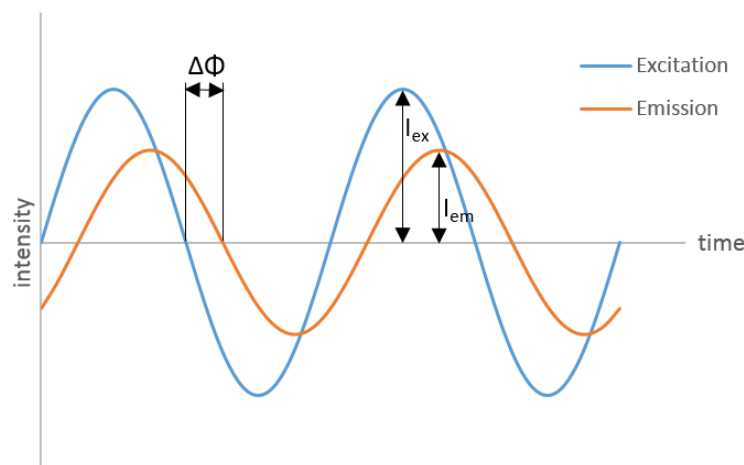


Figure 2.11: Emission and shifted excitation signal at phase fluorimetry

Besides the excitation and emission amplitudes I_{ex} and I_{em} the most important part for dynamically quenched systems is lifetime measurement. In phase fluorimetry, lifetime is

connected to phase shift $\Delta\phi$ or ϕ .

$$\Delta\phi = \arctan \omega\tau = \arctan 2\pi f\tau \quad (2.4)$$

$$\tau = \frac{\tan \phi}{2\pi f} \quad (2.5)$$

$\Delta\phi$...	phase shift
ω	...	circular modulation frequency
f	...	modulation frequency

2.3.4 Single fiber luminescence measurement

There are different ways to measure phase shifts. The basic characteristic of this kind of measurement is if carried out through the sensor or if emission and excitation light are directed in the same path. For the work regarding this thesis a single fiber phase shift measurement device was used.

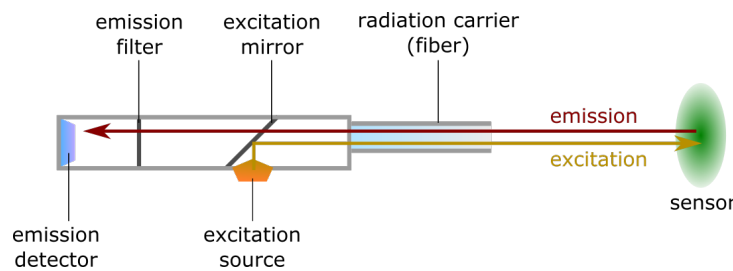


Figure 2.12: Phase shift measurement through a single fiber device

The excitation source emits sinusoidal light that is reflected by a dichroic mirror and then led through a transparent fiber or measurement channel. After excitation, the emitting phase shifted signal is led back to the device through the dichroic mirror. To remove any signal coming from the excitation source, the signal is further processed by a usually long pass filter fitted specially for the emission range. The emission detector records a time dependent signal intensity curve of which the peaks are used to calculate the sensor phase shift.

2.3.5 Dual lifetime referencing - DLR

A special version of phase shift measurement systems is the so called dual lifetime referencing [40]. It is used to convert varying intensity signals of a fluorophore (indicator) into phase shift changes that are measurable with inexpensive phase fluorimetry systems working within a kHz range. Therefore, the overlap of two signals within the same wavelength range is measured, whereas one of the components acts as the reference. Neither phase shift nor intensity of the reference dye can be sensitive to any present analyte. The other signal originates from the indicator dye and varies in intensity due.

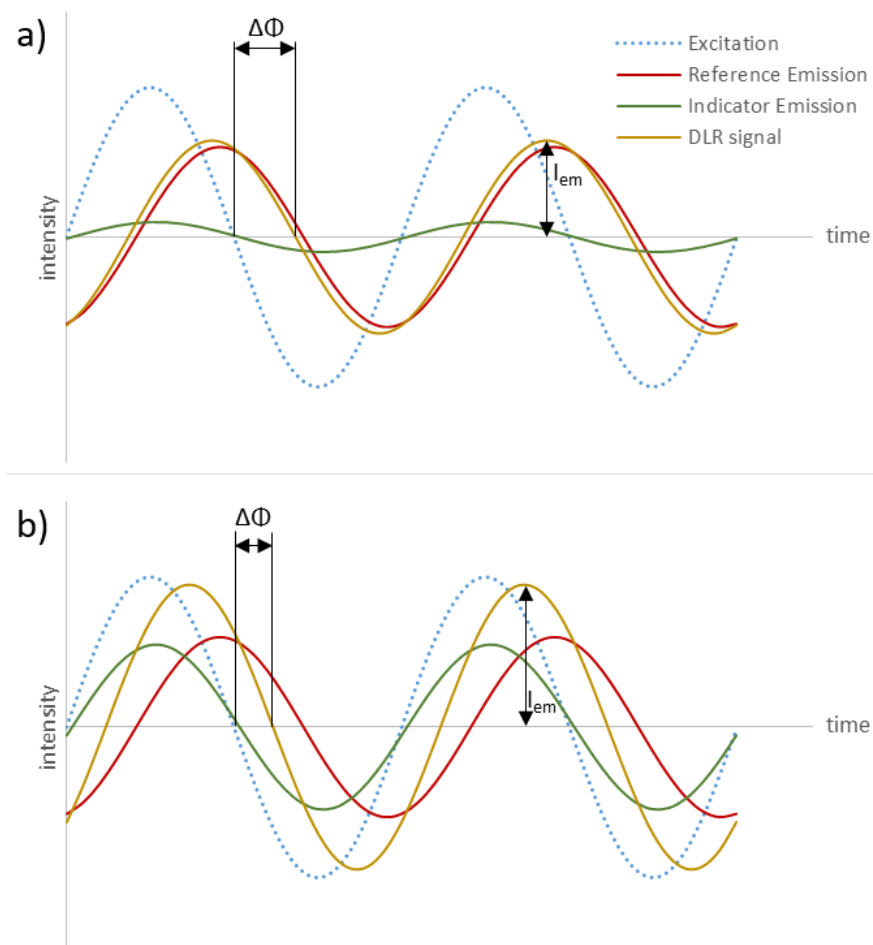


Figure 2.13: Signal development of a DLR system at low and high sensor emission

Figure 2.13 shows the development of a DLR signal. a) demonstrates low and b) higher indicator emission intensities. At shown case the indicator phase shift is not changing at all from a) to b), but the intensity is. The reference signal is constant for both scenarios. This is a crucial characteristic of the referencing dye, since variable phase shifts or intensities would render the reproducibility insufficient. If both dyes are present within the same sensor neither reference, nor sensor emission are measurable individually. The overlapping signal however represents the sum intensity of both emissions. Therefore the measurable intensity not only increases at higher indicator emission, the phase shift also decreases. This way, intensity changes are converted into measurable phase shift calibration systems. A few considerations have to be made for the development of a DLR system:

- emission of both dyes within the same range
- no sensitivity of the reference dye towards present analytes
- dye composition adjustment to gain high phase shift split throughout calibration
- chemical interaction between sensor and reference dye may be problematic

Within this thesis, DLR has been used for pH measurements. Different applications for biocatalytic systems have already shown that the method can be successfully implemented for online pH monitoring in small scale reaction processes [41],[42] and microfluidic devices [30]. Further, DLR sensors for copper ions [5], ammonia [3] and organic compounds in urine [43] have been prepared. Borisov et al. also showed a very interesting use for the DLR system as a multianalyte sensor for simultaneous measurement of CO₂ and O₂ [44].

3 Experimental

3.1 Materials and equipment

In this section the standard equipment and chemicals are listed. Any special devices and adaptations are explicitly stated at the respective chapter throughout the experimental part.

3.1.1 Devices

Manufacturer	Device	Description
VERMES	MDC 3200+	microdispensing control unit
VERMES	MDV 3200A-HS-UF	microdispenser
Benezan Electronics	Triple BEAST	CNC microstep driver
Isert-Electronic	axis motor	step motor for single axis movement

Table 3.1: Sensor printer parts

Manufacturer	Device	Description
Pyro Science	FireStingO2	phase fluorimeter with fiber
Pyro Science	Piccolo2	single system phase fluorimeter
Bruker	Dektak XT	stylus surface profiler
eScope	DP-M01	digital USB microscope
Carl Zeiss	Axiovert 25	microscope
PCO	SensiCam	CCD camera for microscope photography

Table 3.2: Devices used for measurement and recording

Manufacturer	Device	Description
Branson	W-450 D	20 kHz sonification control unit
Branson	102-C Converter	ultrasound converter module
Branson	1/8" Tapered Microtip	metal tip for energy transmission

Table 3.3: Sonifier parts for particle dispensing

3.1.2 Substances

Name	Formula	Distributor
ethyl acetate	C ₄ H ₈ O ₂	VWR chemicals
chloroform	CHCl ₃	VWR chemicals
toluene	C ₇ H ₈	Carl Roth
tetrahydrofuran	C ₄ H ₈ O	VWR chemicals
ethanol	C ₂ H ₆ O	VWR chemicals

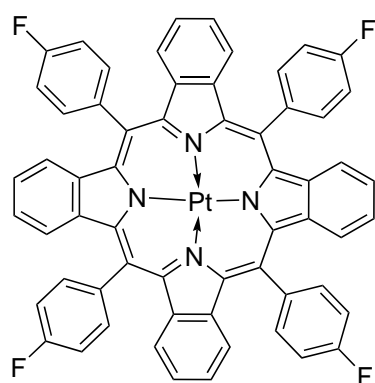
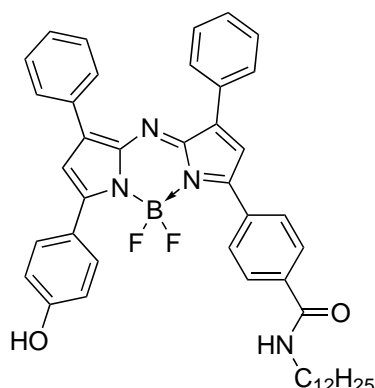
Table 3.4: Solvents used

Name	Formula	Distributor
polystyrene	(C ₈ H ₈) _n	Carl Roth
D4 hydrogel	(ether based hydrophilic urethanes)	AdvanSource

Table 3.5: Polymers used

dye	Trivial Name	Distributor
Pt(II)-meso-tetra(4-fluorophenyl)- tetrabenzoporphyrin	PtTPTBPF ₄	synthesized in house
(Z)-N-dodecyl-4-(5-((5-(4-hydroxyphenyl)-3- phenyl-2H-pyrrol-2-ylidene)amino)-4-phenyl- 1H-pyrrol-2-yl)benzamide	C ₁₂ -OH-aza- BODIPY	synthesized in house
CaCuSi ₄ O ₁₀	Egyptian Blue	synthesized in house

Table 3.6: Sensor and reference dyes used

(a) PtTPTBPF₄(b) C₁₂-OH-aza-BODIPY

3.2 Three axis movement by computerized numerical control (CNC)

The CNC setup used within this master thesis was already installed and ready to use. Prior to the use for microdispensing, it was equipped with an automated airbrush system with fully adjustable valve opening and two relay triggered binary gas valves. These preconditions rendered the setup perfect for the small modifications necessary to carry the microdispensing device.

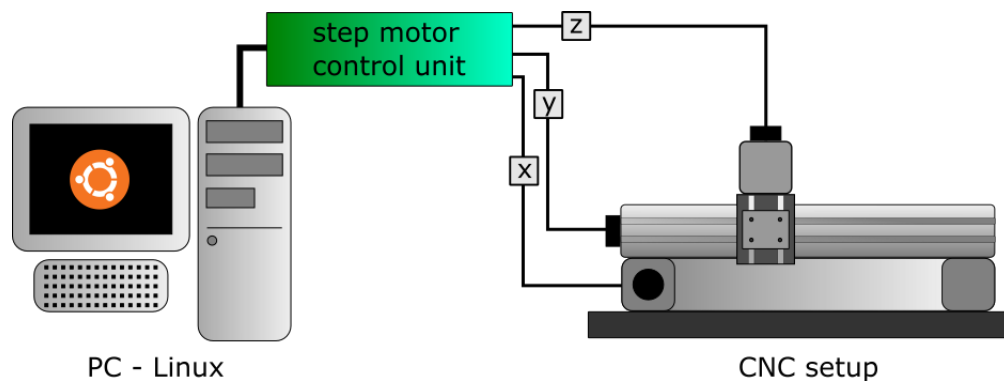


Figure 3.1: Illustration of the CNC setup

The PC runs on Ubuntu and works as the primary operating unit. By using the real time compiling program LinuxCNC the necessary parameters are sent to the step motor control unit. The so called Triple Beast, obtained from Benezan Electronics, is connected to the PC by LPT interface. From there, the signals are given directly to the three step motors (Isert-electronic axis motors).

3.3 Installation of the microdispensing system

The physical attachment of the microdispensing device was carried out by using a specially designed aluminum holding plate. One of the two available relays on the step motor control unit was connected to the trigger PIN of the PLC interface (D-Sub) on the microdispensing control unit VERMES MDC 3200+.

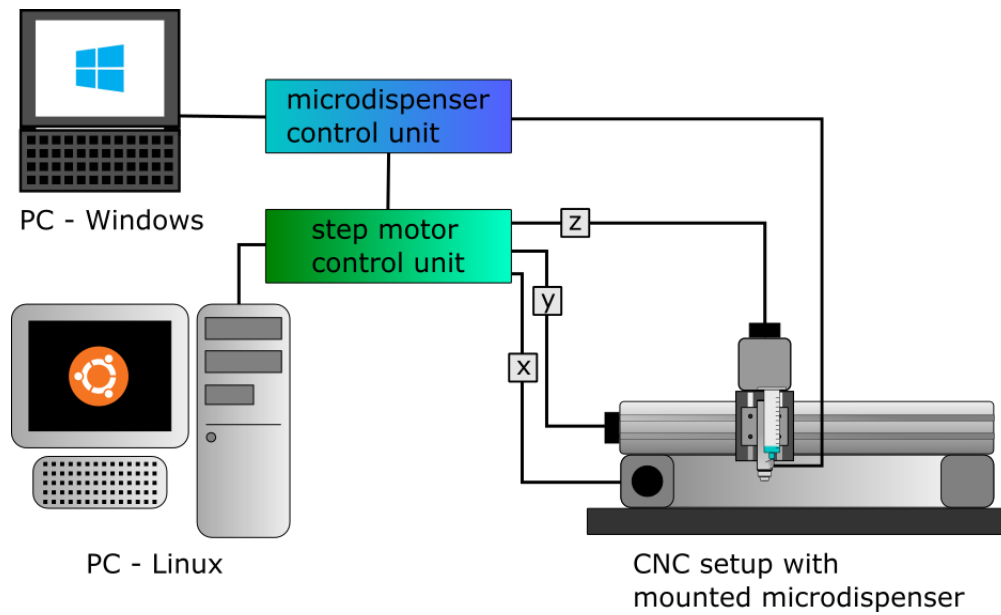


Figure 3.2: Illustration of the completed system

The MDC 3200+ is already equipped with a display and a few buttons for the programming of the microdispensing parameters (see 3.5). Any setup changes however demand a rather time consuming effort. Thus, a Windows PC is connected to the MDC by its RS-232 interface. This is done to provide a faster and more practical alternative for any parameter changes. Finally the microdispenser itself, a VERMES MDV-3200-HS-UF, is connected to the MDC and the system is ready to use.

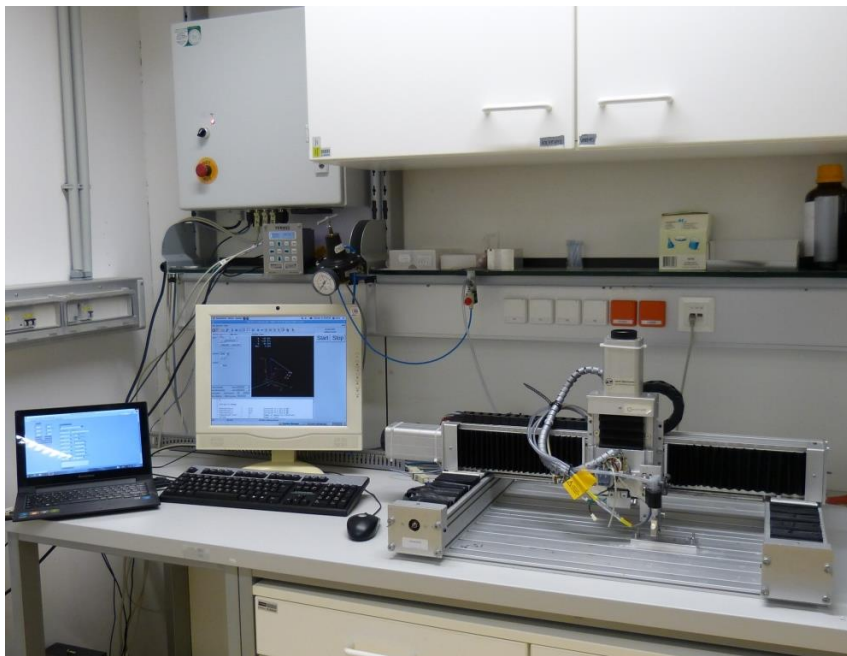


Figure 3.3: Photograph of the completed system

3.4 Provision of a setup interface for microdispensing

The coding part of this thesis is split in two parts. The programming of the microdispenser is carried out with National Instrument's LabView. The three dimensional movement and dispensing triggering is done by the open source CNC machine Controller LinuxCNC.

3.4.1 Movement and triggering - LinuxCNC

Movement is controlled by the CNC program reading a G-code file. This file contains all the information necessary for the controller to execute the demanded movements. Since all printings are carried out in the same pattern, the backbone of said file stays the same. The difference between separate printing files are the variables, that determine the location and number of single spottings.

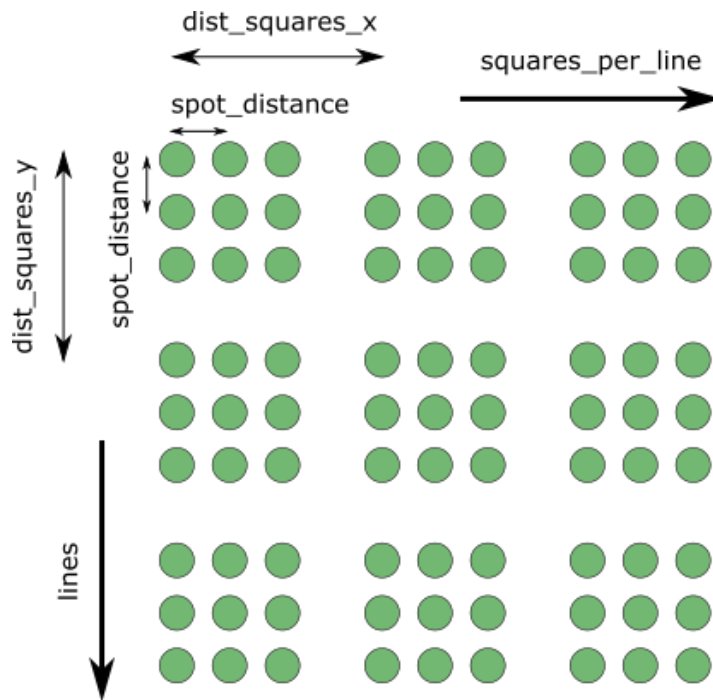


Figure 3.4: Spotting variables illustrated

As illustrated in Figure 3.1, the spotted layers are produced as squares. *squares_per_line* and *lines* determine the number of squares in the respective direction. *square_length* states the number of spots per square. *dist_square* describes the distance between the first spot of two neighbouring squares. If desired the whole process can be repeated with *repeat_count*. A very crucial parameter for the final layer appearance is *spot_distance*, which determines the space between single spots in a square. *move_speed* (usually set to the internal maximum 4000) sets the movement speed in each direction. With *wait_pass* a short interruption can be set between single spottings. *wait_trigger* (usually set to 20ms) represents the time between start and end of the trigger signal, that is sent from the relay to the MDC. Finally, *repeat_clean* and *wait_clean* are used for the cleaning step, that can be set prior to the printing process.

variable	operation
squares_per_line	number of squares in x direction
lines	number of squares in y direction
square_length_y	number of spots per square in y direction
square_lenght_x	number of spots per square in x direction
dist_squares_y	distance between squares in y direction
dist_squares_x	distance between squares in x direction
repeat_count	number of spotting passes overall
spot_distance	distance between single spots within squares
move_speed	axis movement speed
wait_pass	waiting time between spotting and moving
wait_trigger	waiting time between 1 and 0 when triggering
repeat_clean	number of cleaning spots before printing
wait_clean	waiting time between cleaning spots

Table 3.7: Programming variables for the G-code file

A number of "cleaning spots" can be triggered somewhere off the desired substrate to eliminate possible initial complications. To set those parameters for spotting the variables are saved in an ngc file such as:

```

1 #<squares_per_line>=3
  #<lines>=3
  #<square_length_y>=3
  #<square_length_x>=3
  #<dist_squares_y>=2.8
6 #<dist_squares_x>=2.8
  #<repeat_count>=1
  #<spot_distance>=0.6
  #<move_speed>=4000
  #<wait_pass>=0.005
11 #<wait_trigger>=0.02
  #<repeat_clean>=15
  #<wait_clean>=0.05

```

This file is then loaded into LinuxCNC (Figure 3.5), where the machine is homed and, if necessary, the nozzle is aligned. By pressing *Run* the program is then started.

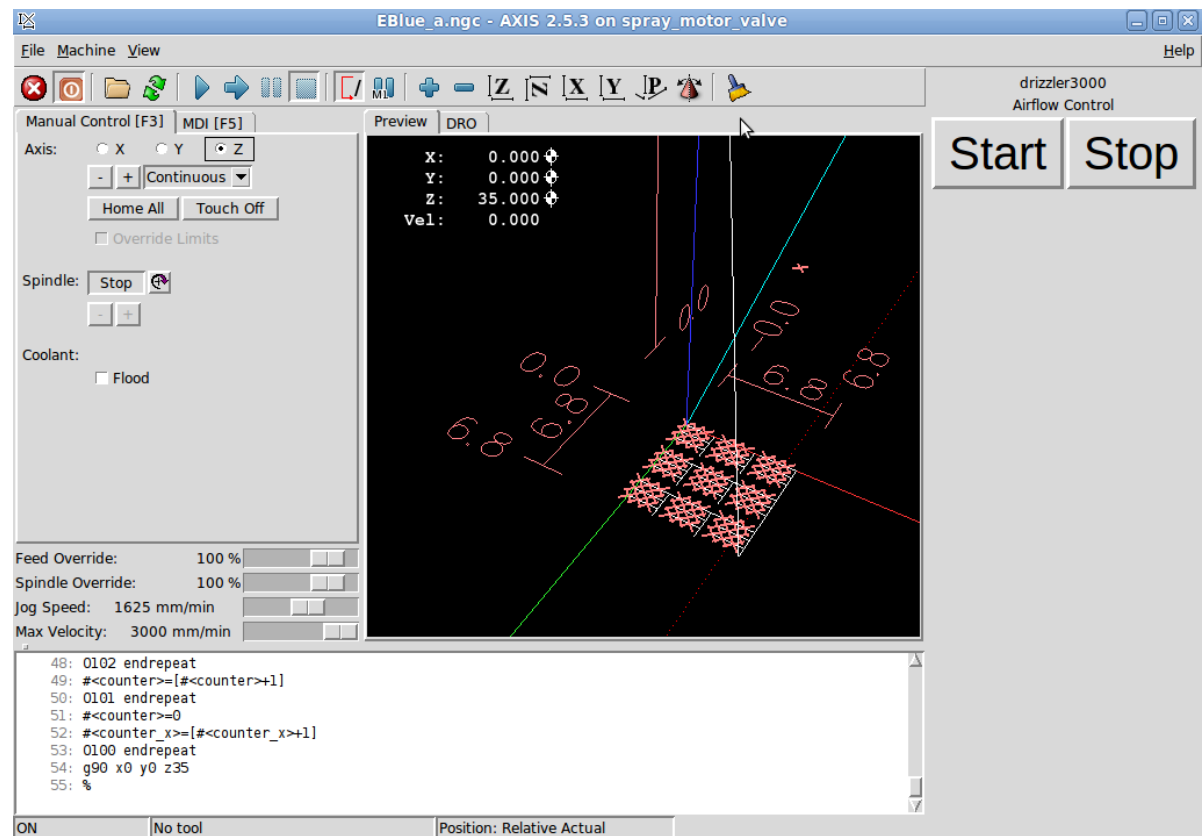


Figure 3.5: Graphic interface of LinuxCNC showing a 3x3 square pattern

3.4.2 Dispensing parameters - LabView

The second programming part is carried out by LabView. The graphic interface consists of two main parts: the internal parameter setting, that is actually communicating with the MDU, and the external parameter mask.

On the left side the six internal parameters can be chosen and sent to the MDU. If the numbers are consistent and within the allowed range of the device, the *Readout* will give back "OK". Otherwise "NAK" is shown as an error. *check system* can be used to examine the parameters that were copied and sent back by the device for verification. These numbers, however will come back as integers, so they carry different potencies than the entered parameters. *Valve up* and *Valve down* can be used to open and close the nozzle manually. With *run program*, the device can be remotely triggered once without a signal from the step motor controlling unit. With *Save settings* and *Load settings* a file containing all six parameters can be saved or loaded directly into the MDU.

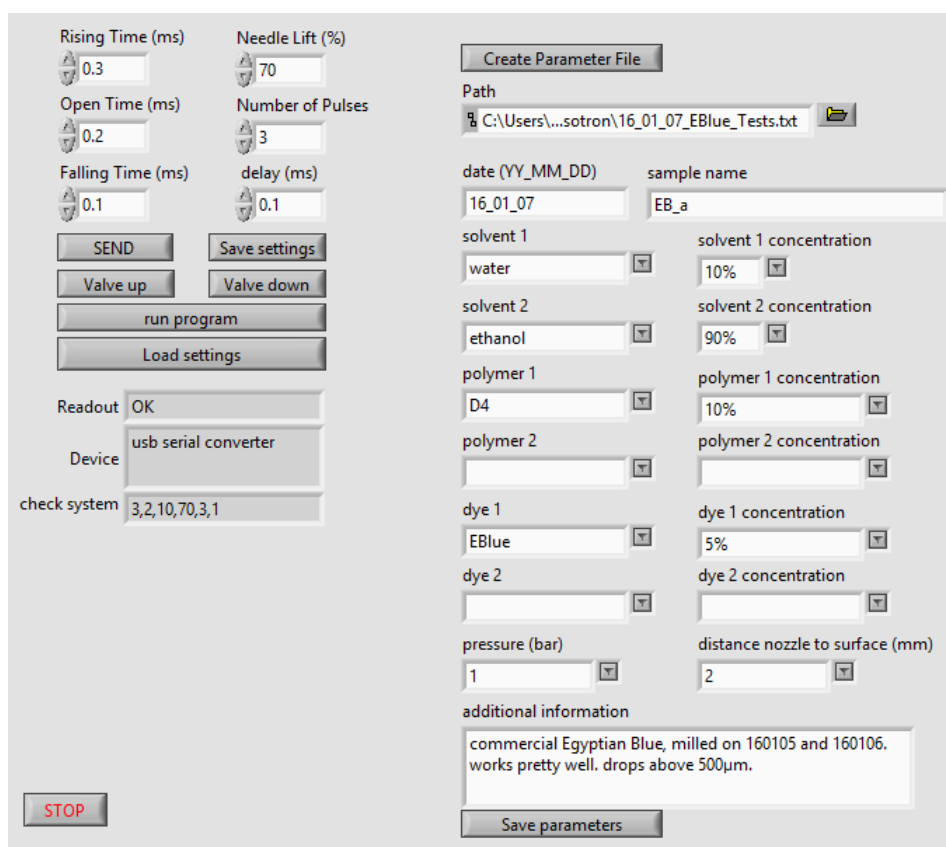


Figure 3.6: Graphic LabView interface: MDU remote control

The right side of the interface contains input possibilities for external parameters such as cocktail composition, pressure and nozzle distance. *Create Parameter File* generates a spreadsheet textfile with one sample (containing all parameters, external as well as internal) per line. *Save parameters* adds a new sample to the file.

3.5 Preparation of polymer layers and spots by microdispensing

The MDS 3200A microdispenser produced by *VERMES* was mounted on a three axis Computerized Numerical Control machine (assembled in-house) run by the freeware *LinuxCNC*. The guiding programs for the dispensing were written in *G Code*. In order to facilitate the setting of parameters, a *LabView* program was created that was able to send predetermined settings to the microdispensing device (RS 232) as well as saving the parameters in a txt file.

The microdispensing device works with a piezoelectrically guided tappet, that “shoots” fluid drops (in this case polymer solutions) through a nozzle. The cocktail reservoir is closed from the outside and under pressure.

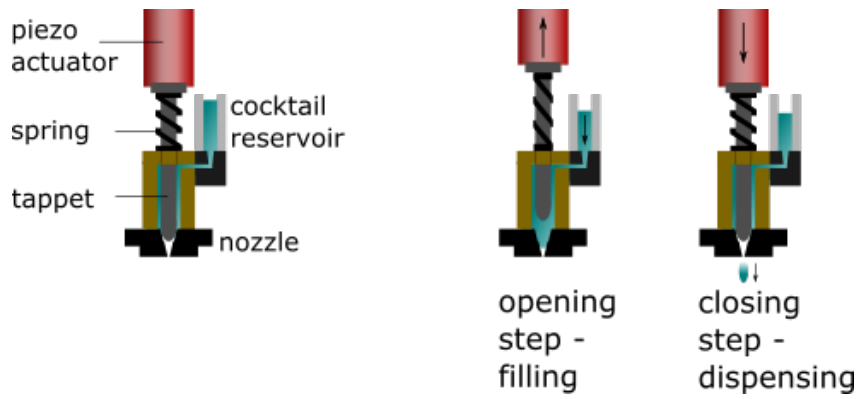


Figure 3.7: Schematic picture of the working principle of a microdispensing device

A single dispensing step is determined by four parameters, which are **rising time**, **open time** and **falling time** as well as the **tappet lift**.

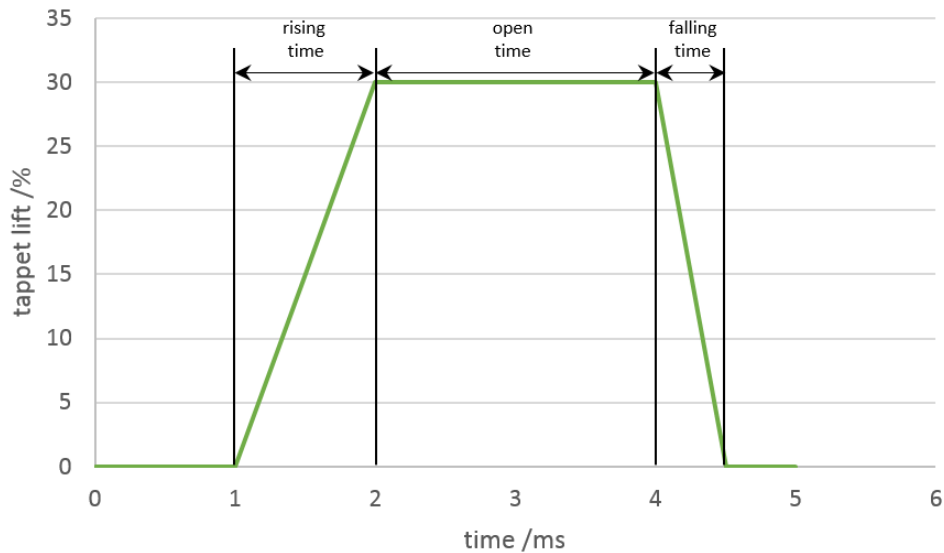


Figure 3.8: Diagram of a single dispensing step; tappet lift vs. time

In the case shown in Figure 3.8, the tappet is opened to 35% lift within 1 ms, stays open for 2 ms and shuts down again in 0.5 ms time span. The opening time was set to minimum in most cases, which ranged from 0.1 to 0.3 ms depending on the tappet lift. The lift itself, as well as the open time, determine the loading process and are changed in order to control the drop volume. The falling time determines the falling energy, leading to higher droplet speeds at lower falling times.

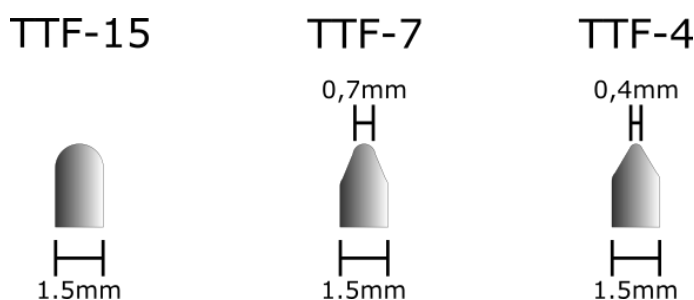
Besides those four internal dispensing parameters, a set of five further characteristics are rather important for the overall appearance of the dispensed spot (Table 3.8).

Pressure and viscosity are two further parameters that affect the drop volume. The system is designed to work with pressures ranging from 0-7 bar and viscosities up to 2000 Pas. Both parameters are usually correlated to each other, leading to increasing container pressure at higher viscosities in most cases. The particle size may be a very delicate topic, especially for

Parameter category	Parameters
Cocktail	Viscosity Boiling point (solvent) Particle size (if apparent)
Microdispenser, external	Container pressure Distance nozzle - substrate
Microdispenser, mechanical	Nozzle diameter Tappet tip diameter
Printing process	Spot distance

Table 3.8: Crucial parameters for dispensing

higher particle sizes and/or materials that tend to agglomerate. The use of particle dispersions very often leads to the need of higher nozzle diameters to prevent clogging. The solvent boiling point or respectively its partial pressure at working temperature (usually 22°C) affects two important dispensing characteristics. On one hand, higher partial pressures may lead to unwanted polymer precipitation on the nozzle surface due to the fast solvent evaporation. On the other hand is the behaviour of the dispensed spot/layer heavily reliant on the evaporation speed after application. If the cocktail tends to form coffee rings, faster evaporation may be fortunate. The nozzle diameter, ranging from 50 μm to 600 μm in our system, correlates to the drop volume. For producing sensor layers in microfluidic systems, it is preferred to find the smallest possible nozzle, but as mentioned previously this is often limited by particles. The distance between nozzle exit and substrate has a small influence in the impingement energy. Larger distances slightly slow the cocktail drop on its way to the surface and also give it more time for solvent evaporation during the fall. Last but not least, the tappet diameter also determines the drop volume. For the description nomenclature of the tappet, VERMES has a systematic concept: CTF stands for ceramic tappet material, whereas TTF tappets are made out of Tungsten. The number afterwards describes the diameter of the tip. Narrower tips lead to a tighter closing and leave less volume for filling.

**Figure 3.9:** Schematic presentation of different tappet sizes

The first strategy to prepare polymer spots was to produce single spots in sizes mostly above 1 mm. This step was done to evaluate the best possible spotting parameters and cocktail compositions for the microdispensing process. Afterwards, the spot size was decreased and layers were printed by close arranging of smaller spots (usually around 500 μm). The spot size

is the crucial parameter that determines the resolution of the finished layers.

After the change from single spot to printing arrays, spot distance was introduced as new parameter. Depending on the spot volume, its viscosity and the surface interaction between substrate and cocktail, the distance between single spots – respectively pixels – had to be adjusted.

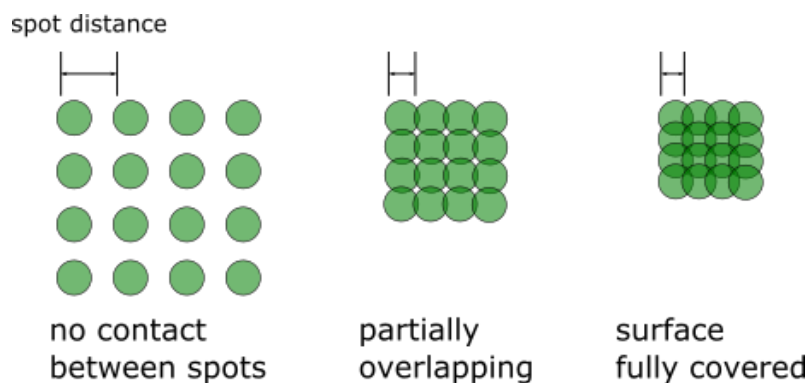


Figure 3.10: Different methods of sensor printing

3.6 Determination of the influence of different parameters on spot appearance

Different sets of cocktails and spots were created by using different spotting parameters. The experiments aimed at finding cocktail compositions that were suitable for creating homogenous, flat polymer layers in different thicknesses and spot sizes. In hindsight for future oxygen sensor layers, polystyrene (MWaverage: 260.000 Da) was used for those tests. For better visibility the polystyrene cocktails also contained 0.25% or 1% macrolex red dye. As solvents chloroform, ethyl acetate, toluene and tetrahydrofuran were used, either pure or in mixtures of two. The forgoing cocktail preparations were chosen by the outcome of previous sensor layers. Therefore, some "rules" were applied for ongoing parameter changes (Table 3.9).

Spotting issue	Parameter change
Coffee ring	Increase viscosity (higher polymer concentration) Decrease falling energy Decrease evaporation time (lower boiling point of solvent/solvent mixture)
Drop formation on nozzle	Increase evaporation time (higher boiling point of solvent/solvent mixture) Decrease viscosity (lower polymer concentration) Increase falling energy
Splattering on substrate	Increase viscosity (higher polymer concentration) Decrease falling energy

Table 3.9: Necessary parameter changes for unwanted spotting issues

The experiments aimed at evaluating the impact of parameter changes on the appearance of the spot regarding colour intensity (which is related to the layer thickness), spot size, spot shape and coffee ring. All spots were prepared with a TTF-15 tappet and 50 μm nozzle size. The most exemplary spots are listed in 4.1.

3.7 Reference particle dispersing

The reference material for pH sensors - Egyptian Blue - tends to form agglomerates during dispensing. Since nozzle diameters of the microdispenser go down to 50 μm , bigger fragments could possibly clog the system partly or fully, leading to significantly lowered reproducibility in sensor printing. In order to find a suitable redispersing method for Egyptian Blue powder, four different cocktails were prepared.

Cocktail	Solvent	w(EB) /%	w(D4) /%
THF6	THF	6	6
THF10	THF	10	10
EtOH6	ethanol(9)/water(1)	6	6
EtOH10	ethanol(9)/water(1)	10	10

Table 3.10: Cocktails prepared for dispensing tests

The cocktails were chosen with different solvent polarities (THF as unpolar and ethanol/water as polar solvent) in order to find out if there are differences in dispersion stability. Further, for both solvents two different polymer concentrations of D4 were used (6% and 10%) for lower and higher viscosity, which should play an important role regarding particle sedimentation. For the experiment 2 ml of each cocktail was transferred into a 4 ml glass vial. First, the mixtures are magnetically stirred for 10 minutes. 50 μl are applied on a microscope glass slide for optical evaluation under the microscope. Then, the vials containing the stirred cocktail are left on the bench for the sedimentation process. Afterwards the cocktails are dispersed with the Sonifier 250 from Branson Ultrasonics Corporation. For the energy transfer a 3,175 mm microtip was used. To prevent overheating during the dispersing, a rather high pause time between sonification pulses was set up.

Parameter	Description	Value
energy	ultrasonic energy in percent	25%
runtime	overall sonification time	15 s
pulse on	sonification time per cycle	1 s
pulse off	pause time between cycles	9 s

Table 3.11: Sonification parameters for Egyptian Blue dispersing

After sonification, another set of microscope samples was taken and the sedimentation process of 10 minutes was repeated including taking pictures afterwards.

3.8 Evaluation of dispensing reproducibility

In order to get information about the stability of large sets of dispensed single spots and layers, oxygen and pH sensors were prepared on polymer microscope slides. Every single sensor was then calibrated to get data for phosphorescence lifetime and luminescence intensity. For the pH sensors it was also necessary to find a fitting dispensing technique, since agglomerations of the respective reference particles would lead to severe nozzle clogging. In the end, the results should give more information about potential improvements for the overall printing process to get reproducible results.

3.8.1 Preparation of multiple sensor spots and layers on PMMA slides

For pH as well as for oxygen sensors PMMA slides were printed with the respective sensors in different sizes and layer thicknesses. Small sensor spots in the range of 400 μm were made in sets of 152 spots per slide (19 spots per line, 8 lines), whereas 48 square layers (3x3) were done in 4 lines.

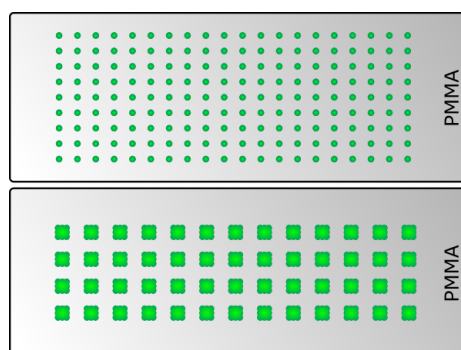


Figure 3.11: Scheme of prepared sensor slides, 8x19 for small spots and 4x12 for square layers

Both cocktails consisted of around 8% polymer and 0,5% indicator dye ($w_{dye/pol}$). The pH cocktail also contained the same amount of Egyptian Blue as D4 hydrogel. The exact compositions of the cocktails are given in Table 3.12.

	Oxygen sensor	pH sensor
solvent	THF(1)/toluene(1)	ethanol(9)/water(1)
polymer	8% polystyrene MW: 260k	7.5% D4 hydrogel
dye 1	0.04% PtTPhTFBP	7.5% Egyptian Blue
dye 2		0.0375% pH-sensitive dye

Table 3.12: Cocktail compositions for the reproducibility tests

Before printing, the pH cocktail was sonified with the same program that was tested out earlier for the dispersing experiments (see Table 3.11). For each cocktail one global dispensing setup was used for the single spots as well as for the square layers. In addition to the varying sensor sizes, also different layer counts were produced. For each sensor and size two slides were prepared with one pass and three passes of the printing process. After printing, the slides were dried in an oven for 90 minutes at 60°C.

	Oxygen sensors	pH sensors
pressure	0.8 bar	0.6 bar
distance	0.8 mm	0.5 mm
tappet lift	45%	40%
rising time	0.2 ms	0.2 ms
open time	0.1 ms	0.1 ms
falling time	0.2 ms	0.2 ms
spot distance - single spots	2 mm	2 mm
spot distance - squares	0.35 mm	0.3 mm
square distance	4 mm	4 mm

Table 3.13: Dispensing parameters for the reproducibility tests

3.8.2 Automated evaluation readout system

For the oxygen sensors the evaluation was done with the slides submerged in water (calibration for aerated sensor) or 2% Na₂SO₃ solution (deaerated). The pH slides were calibrated in three buffer solutions.

pH	Buffer	Ionic strength
3,8	CH ₃ COOH 25mM	NaCl 100mM
7,7	NaH ₂ PO ₄ 25mM	NaCl 100mM
10,5	CAPS 25mM	NaCl 100mM

Table 3.14: Buffer solutions for pH calibration

The readout of the sensors was automatized. Therefore, the microdispenser was removed and the phase shift measurement systems were mounted onto the CNC head of the machine. For the oxygen sensors a polymer fiber (diameter 1 mm) connected to a FireStingO₂ was used. For the pH system, especially for the single spots, the signal intensity was too low while using a 1 mm fiber. Therefore, a Piccolo₂ was mounted directly to the system. Due to the rather small spot sizes and the sensible readout system, physical shifting of the slide during measurement would have been a major problem, especially regarding signal intensity. To prevent the system from any offset during the measurement, a magnetic support was introduced into the basin.

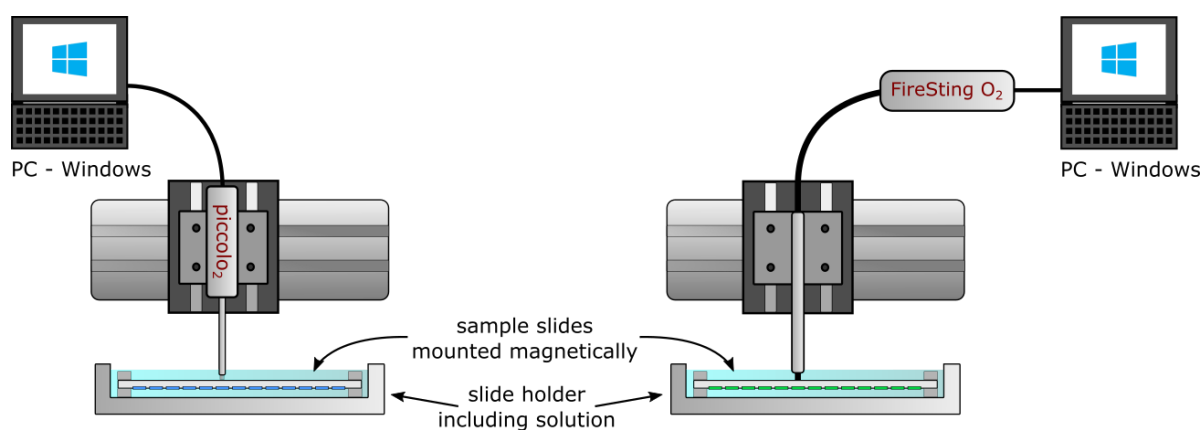


Figure 3.12: Automated phase shift readout system

The Firesting and Piccolo were set up to 100% excitation intensity and background-calibrated. The values were recorded with a measurement frequency of 0.7 s (Firesting) and 0.5 s (Piccolo). To facilitate the evaluation, the CNC program was written in a way to measure 3 to 5 times per spot/layer and then at least two zero values in between. That way, a specially written python program was able to distinguish related signals and select intensity and phase shift and intensity for each sensor automatically.

3.9 Preparation of multilayer pH sensors

To demonstrate the ability of the microdispensing system to produce sensors with multiple layers, a pH sensor was created with a different approach than using single-cocktail preparation. The goal was to prepare Egyptian Blue layers and add different amounts of indicator layers on top to produce several sensors that should show increased signal split with higher amounts of sensor.

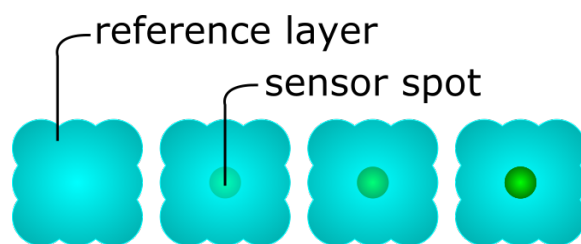


Figure 3.13: pH layer sensor with different amounts of sensor dye

Contrary to the usual pH sensors, the Egyptian Blue was not implemented into D4 as a matrix, but in polystyrene to ensure the adhesion. After 60 minutes of drying at 60°C the pH sensitive dye (D4 as matrix) was then printed on top. This was done in printings of two from 0 to 22 dispensing steps per spot. Another 60 minutes of drying at 60°C completed the production process.

	Reference layer	pH sensitive layer
solvent	THF(1)/toluene(1)	THF(7)/toluene(3)
polymer	6% polystyrene MW: 260k	2% D4 hydrogel
dye 1	6% Egyptian Blue	0.06% pH-sensitive dye

Table 3.15: Cocktail compositions for the pH layer sensors

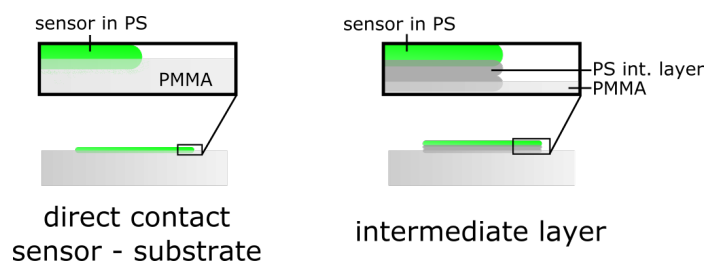
	Reference layer	pH sensitive layer
pressure	0.6 bar	0.2 bar
distance	0.5 mm	1 mm
tappet lift	40%	33%
rising time	0.2 ms	0.1 ms
open time	0.1 ms	0.1 ms
falling time	0.2 ms	0.03 ms
spot distance - squares	0.35 mm	-

Table 3.16: Dispensing parameters for the pH layer sensors

For the evaluation of the produced layer sensors the same setup as in 3.8.2 was used with pH values of 3.8, 7.7 and 10.5.

3.10 Preparation of intermediate layers for dye migration prevention

Since sensor printing is not only done on glass substrates but also on polymer materials, material exchange between sensor cocktail and substrate is inevitable at some point. Especially when high boiling solvents such as toluene are involved, the droplet takes significantly longer to dry out and starts to dissolve the surface of the polymer carrier. Within this process dye molecules migrate from the originally intended matrix into the substrate material, where the sensor behaviour can be influenced heavily.

**Figure 3.14:** Schematic illustration of printed sensors with and without intermediate layers

The solution to this problem was carried out in two steps: a) finding the right parameters for intermediate layer printing and b) figuring out the necessary height of intermediate layers to eliminate the problem.

3.10.1 Preparation of intermediate layers with varying thicknesses

Four sets of 4x4 matrix layers were printed on PMMA with different heights from 1 to 15 passes. As the only varying parameter the spot distance was set up from 260 μm to 320 μm in 20 μm steps.

solvent	THF(7)/toluene(3)
polymer	8% polystyrene MW: 260k

Table 3.17: Cocktail compositions for printing intermediate PS layers

pressure	0.2 bar
distance	0.7 mm
tappet lift	30%
rising time	0.2 ms
open time	0.1 ms
falling time	0.03 ms
spot distance - squares	0.26-0.32 mm

Table 3.18: Dispensing parameters for printing intermediate layers

After layer preparation the slide was dried at 60°C for 1 hour. For height profile evaluation a BRUKER Dektak XT was used and a straight line through the center of the layer was measured.

3.10.2 Sensor printing on intermediate layers

After evaluation of the intermediate layer profiles the most suitable ones were used for printing 3x3 sensor layers on top. Additionally, one sensor layer was printed directly on top of the PMMA slide to have a signal reference for no intermediate layer.

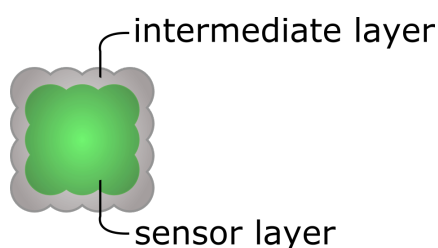


Figure 3.15: Sensor centered on an intermediate layer

solvent	THF(7)/toluene(3)
polymer	8% polystyrene MW: 260k
dye	0.04% PtTPhTFBP

Table 3.19: Cocktail compositions for printing oxygen sensors on PS intermediate layers

Consisting of the same characteristics apart from sensor dye, the same dispensing parameters were used to dispense the sensor cocktail as in Table 3.18. After drying for 1 hour at 60°C the sensor was ready for evaluation. The slide was immersed in water at 25°C and the signal was measured with a 1 m fiber connected to a FireSting at 100% excitation intensity and 400x signal amplification.

4 Results and Discussion

Different polymer solutions were prepared and spotted with varying parameters to evaluate the importance and effect on spot appearance. Selected pictures of conclusive sets of spots are shown and discussed in this section.

4.1 Determination of the influence of different parameters on spot appearance

4.1.1 Tappet lift

The tappet lift was assumed to be one of the most important parameter regarding drop volume. Naturally, higher tappet lift leads to increased volume during the loading step and therefore is a useful tool for dropsize adjustment. However, the range of tappet closing, respectively the falling time, is also affected by different tappet lifts. Increasing lift settings lead to higher minimal falling times.

tappet lift /%	1-10	11-20	21-30	31-40	41-50	51-60	61-70	71-80	81-90	90-100
min. falling time /ms	0.01	0.02	0.03	0.04	0.05	0.06	0.07	0.08	0.09	0.10

Table 4.1: Lowest possible falling times

Nonetheless, due to the nature of the electromechanical behavior of the piezo actuator (extension acceleration), higher falling energies are achieved at higher lifts. A set of spots have been prepared to show the influence of different tappet lifts.

solvent	toluene
polymer	PS 6%
dye	macrolex red 1%
pressure	0.6 bar
distance	2 mm
rising time	0.2 ms
open time	2 ms

Table 4.2: Dispensing parameters for PS.6.tol_lift_2 150805

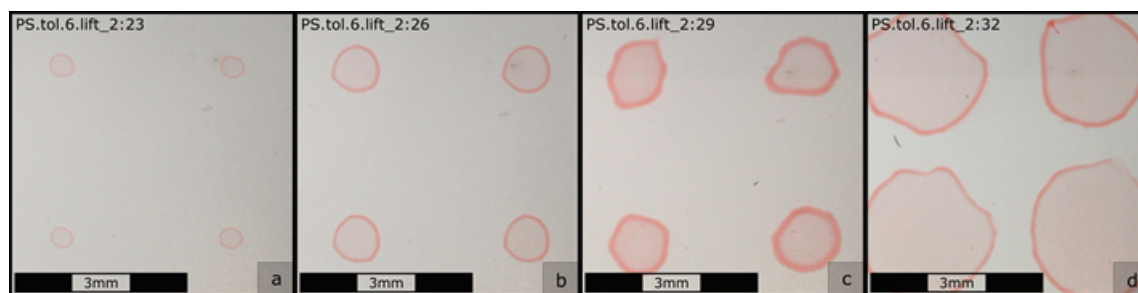


Figure 4.1: PS.6.tol_lift_2: spots prepared with varying tappet lifts and minimum falling time; lift/falling time: a(23%/0.03 ms), b(26%/0.03 ms), c(29%/0.03 ms), d(32%/0.04 ms)

solvent	toluene
polymer	PS 6%
dye	macrolex red 1%
pressure	0.4 bar
distance	2 mm
rising time	0.2 ms
open time	15 ms

Table 4.3: Dispensing parameters for PS.6.tol_lift_3 150805

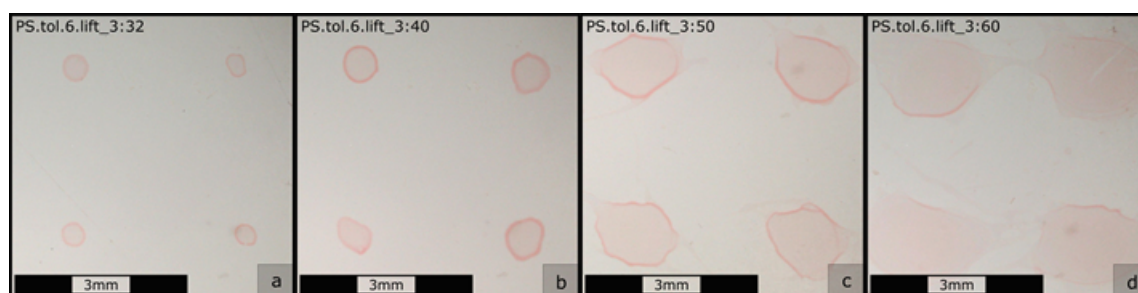


Figure 4.2: PS.6.tol_lift_3: spots prepared with varying tappet lifts and minimum falling time; lift/falling time: a(32%/0.04 ms), b(40%/0.04 ms), c(50%/0.05 ms), d(60%/0.06 ms)

The two spotting sets PS.tol.6_lift_2 and PS.tol.6_lift_3 are shown because it shows a rather typical characteristic of increased tappet lifts. At 0.6 bar and 2ms open time, there is a huge increase in spot size between 23% (350 μm) and 32% (2200 μm). However, within this narrow range of lift change there is no heavily significant difference in appearance besides the spot size. The coffee ring remains and there is always at least the indication of a circular spot, even if the outline starts to aberrate at higher lifts. The second presented row of spots was prepared with less pressure but higher open times to get information about highly differing tappet lifts without overloading the system. As it can be seen, the increase in spot size is similar to the set shown prior, but the development of appearances of the spots regarding coffee ring and shape is different. Whereas the circular characteristic is still visible up to 40% lift, at 50% and 0.05ms falling time the produced polymer spot seems rather undefined. It appears that the drop was applied with high energy, leading to a flatter and less defined structure. The

smaller coffee ring also supports this conclusion, since the small height of the applied cocktail would lead to faster evaporation and therefore less time for coffee ring formation. At 60% and 0.06 ms this effect is visible even better. The following can be concluded:

- As expected, higher tappet lifts lead to increased spot volume. The increased loading volume as well as the larger opening profile between nozzle and tappet creates a higher load during the same open time.
- The minimum falling times for each tappet lift do not have equal exit energies. 0.6 ms at 60% for example creates a higher falling energy as 0.1 ms at 10%. This effect is caused by the piezoelectric behavior of the actuator, which has a certain acceleration during its expansion.

4.1.2 Falling time

To show the effect of different falling times at constant tappet lifts two experiments are shown with different solvents. The first one was performed with a 12% polystyrene cocktail dissolved in a toluene/chloroform mixture (4+1). The rather viscous solution was applied with highly differing falling times at 60% tappet lift.

solvent	toluene (4) + CHCl ₃ (1)
polymer	PS 12%
dye	macrolex red 0.25%
pressure	1.0 bar
distance	2 mm
rising time	0.5 ms
open time	0.5 ms

Table 4.4: Dispensing parameters for PS.12.tol.80.chlor.20_fall_2 150810

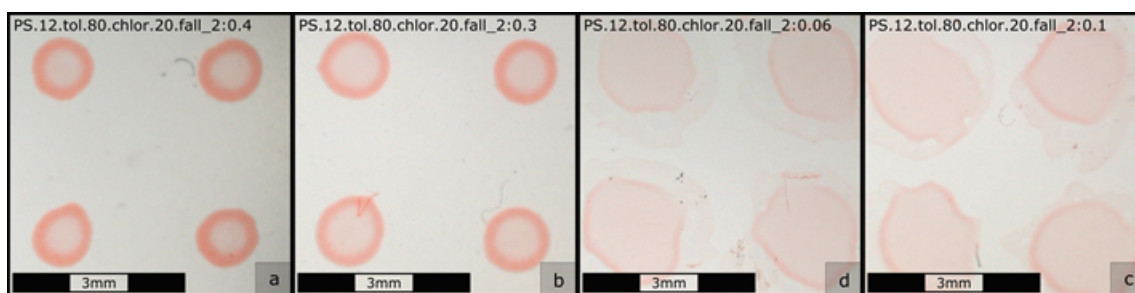


Figure 4.3: PS.12.tol.80.chlor.20_fall_2: spots prepared with varying falling times; lift/falling time: a(60%/0.40ms), b(60%/0.20ms), c(60%/0.10ms), d(60%/0.06ms)

Based on presented spot appearances it seems that reduced falling time has similar effects to increased tappet lift. The difference in this case however is that the flatter and more undefined spots are created at less drop volumes, since the faster tappet closing reduces the overall loading time. It can be seen that between 0.40 ms and 0.20 ms there is a significant increase in spot size from about 1.0 mm to 1.3 mm. Between spots prepared with 0.06 and 0.10 ms there is no distinct difference in appearance visible. Both lack circular shape and heavy coffee ring formation. The

second set shown was prepared with ethyl acetate instead of a toluene/chloroform mixture, to get information about the behaviour of spots containing faster evaporating solvents.

solvent	ethyl acetate
polymer	PS 15%
dye	macrolex red 0.25%
pressure	1.0 bar
distance	2 mm
rising time	0.2 ms
open time	0.1 ms

Table 4.5: Dispensing parameters for PS.15.EtOAc_fall_1 150817

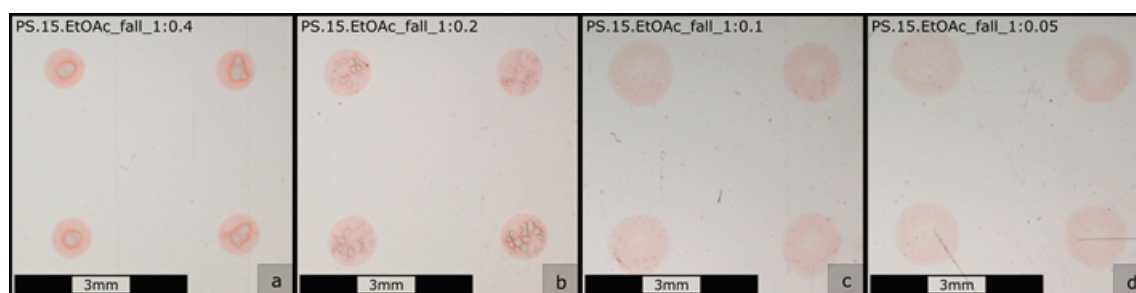


Figure 4.4: PS.15.EtOAc_fall_1: spots prepared with varying falling times; lift/falling time: a(50/0.40ms), b(50/0.20ms), c(50/0.10ms), d(50/0.05ms)

The most apparent difference to the previously shown pictures is the appearance of the spots with lower falling energies. Instead of the formation of defined and uniform coffee rings, at 0.40 ms and 0.20 ms falling time clearly visible bubble inclusions occur. Whereas 0.40 ms delivers spots with single bubbles of around 350 μm within the 700 μm spot, 0.20 ms leads to the formation of a set of smaller blisters in the range of 100 μm throughout the whole layer. This effect disappears at 0.10 ms, where the spot forms a gradual polymer distribution in its radial direction. Instead of a clear coffee ring, it shows steadily decreasing intensity from outside to center. The same behavior can be observed at the minimum falling time of 0.05ms with slightly increased coffee ring behavior. To summarize, the following observations could be made for the influence of different falling times:

- The falling time has a very significant impact on the ratio between layer thickness and spot diameter. Lower falling times (higher falling energies) lead to increased diameters and lower layer thicknesses.
- For cocktails containing solvents with higher partial pressures, the falling time plays an important role regarding the formation of air pockets or blisters. Due to the fast evaporation, thicker layers tend to form bubble inclusions rather than ordinary coffee rings. This effect can be minimized by reducing the layer thickness and therefore lower falling times.

4.1.3 Pressure

To get information about the influence of loading pressure, different sets of experiments with same internal parameters were performed, adjusting only the reservoir pressure. Below two rather descriptive sets with the same cocktail were chosen to be presented.

solvent	toluene
polymer	PS 6%
dye	macrolex red 1%
tappet lift	40%
distance	2 mm
rising time	0.2 ms
open time	0 ms
falling time	0.04 ms

Table 4.6: Dispensing parameters for PS.6.tol_pressure_1 150805

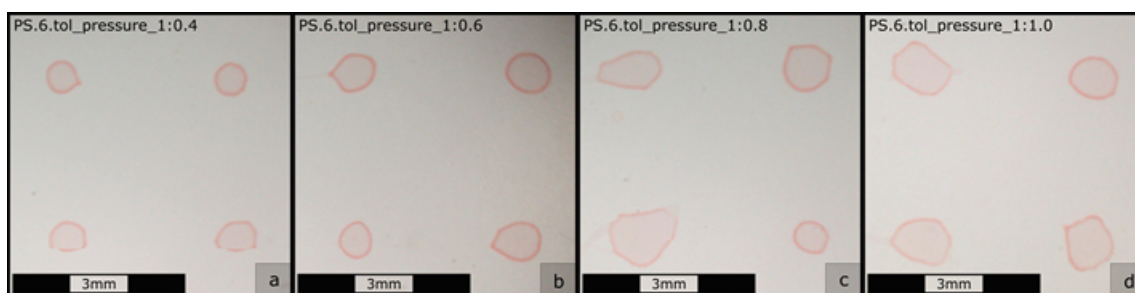


Figure 4.5: PS.6.tol_pressure_1: spots prepared with varying reservoir pressures; pressure: a(0.4bar), b(0.6bar), c(0.8bar), d(1.0bar)

The first experiment shown leads to the conclusion that higher pressure increases the drop volume. This effect is most likely originating in increased force on the cocktail surface within the reservoir that would accelerate the loading process at the same opening volumes. However, the next set show slightly different behavior regarding increased reservoir pressures.

solvent	toluene
polymer	PS 6%
dye	macrolex red 1%
tappet lift	25%
distance	2 mm
rising time	0.2 ms
open time	15 ms
falling time	0.03 ms

Table 4.7: Dispensing parameters for PS.6.tol_pressure_2 150805

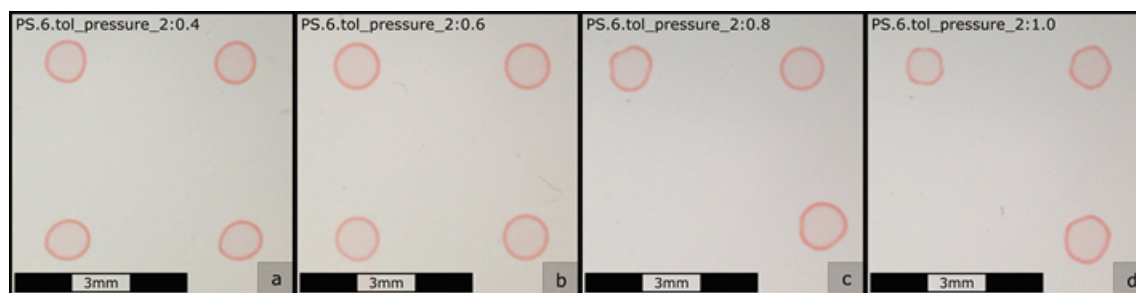


Figure 4.6: PS.6.tol_pressure_2: spots prepared with varying reservoir pressures; pressure: a(0.4 bar), b(0.6 bar), c(0.8 bar), d(1.0 bar)

At lower tappet lifts the influence of pressure seems to decrease drastically. Visual evaluation of the spots feature almost no change in spot size and intensity between 0.4 bar and 1.0 bar. This may be caused by the significantly lowered cross sectional area for loading. The rather unexpected phenomenon was the loss of single spots at 0.8 bar and 1.0 bar. For both experiments 2 out of 18 spots were not dispensed at all and led to increasing drop formation on the nozzle. Thus, the important observations for different pressures are as follows:

- Given a tappet lift high enough, the pressure significantly increases the drop volume. Besides the opening time it is an important parameter for drop size adjustment. However, considering the effort of manual pressure changes, it seems to be better to adjust the pressure once to fit the viscosity of the cocktail and leave it constant afterwards.
- The pressure seems to have decreased influence at lower tappet lifts. This effect must be considered for the preparation of very small spots as to reduce the risk of heavy drop formation on the nozzle.

4.1.4 Distance

For flat substrates it is possible to adjust the distance between nozzle and substrate at will. For complex structures such as microreactors or microplates for example it is necessary to increase the distance. As can be seen in Figure 4.7 there are small differences in the appearance of dispensed spots.

solvent	toluene (4) + CHCl_3 (1)
polymer	PS 12%
dye	macrolex red 0.25%
tappet lift	36%
pressure	1.0 bar
rising time	0.5 ms
open time	0.5 ms
falling time	0.10 ms

Table 4.8: Dispensing parameters for PS.12.tol.80.chlor.20_distance_1 150810

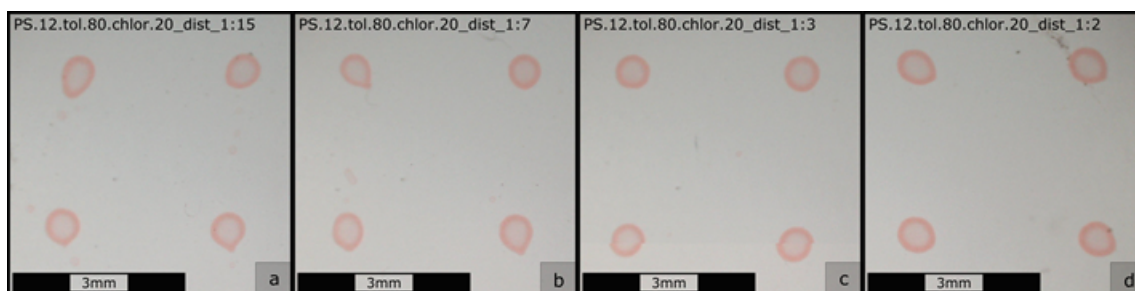


Figure 4.7: PS.12.tol.80.chlor.20_distance_1: spots prepared with varying substrate-nozzle distances; distance: a(15 mm), b(12 mm), c(3 mm), d(2 mm)

The alignment, as well as the appearance of the spots at 7 mm and 15 mm differs from the one at standard distance (2 mm). The most obvious explanation for this observation would be a tilted falling path. During the spotting process polymer precipitation can occur on the nozzle, which leads to a deflection of the falling drop. It can finally be concluded:

- If possible, working near the substrate (<2 mm) is advised. Working with higher distances leads to disalignment of the spots during the ongoing dispensing process. This effect will most likely play an even bigger role when working with particles (increased risk of clogging) and lower boiling solvents (faster evaporation on nozzle).

4.2 Egyptian Blue dispersing

As reference material for the pH sensor long-lasting dispersing of Egyptian Blue plays an important role for reproducible sensor production. This short section covers the effects of classical magnetic stirring and ultrasonic dispersing on reference cocktails.

It was immediately apparent, that redispersing of Egyptian Blue just by magnetic stirring was not suitable for a homogenously suspended cocktail. Even after agitating with a lab vortexer, big chunks of agglomerates were easily visible by eye.

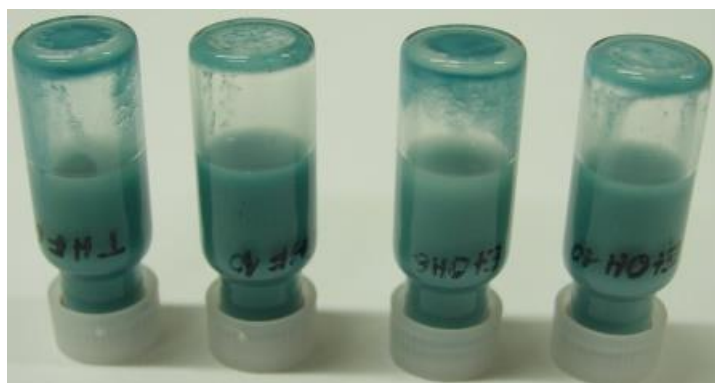


Figure 4.8: EB cocktail after 10 min stirring; from left: THF 6, THF 10, EtOH 6, EtOH 10

Interestingly no heavy difference in sedimented amount of particles can be made out between different solvents. The polymer concentration however shows a very important role, as expected. Obviously, sedimentation is significantly lower at higher polymer concentrations. For the sonified cocktails a substantial increase in cocktail quality was expected.

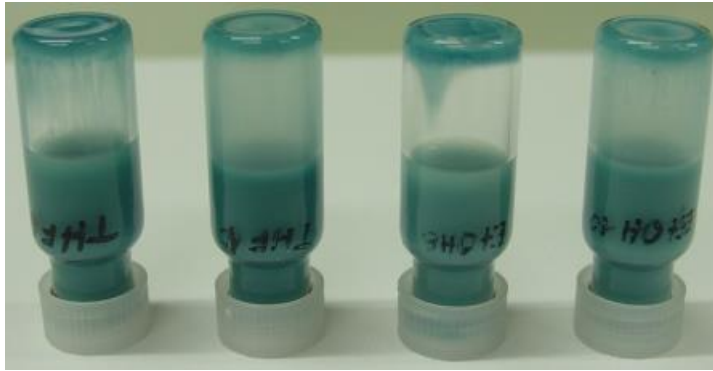


Figure 4.9: EB cocktail after 15 s sonification; from left: THF 6, THF 10, EtOH 6, EtOH 10

After sonification, the major part of bigger agglomerates vanished and the overall cocktail quality appeared to improve drastically. Microscopic images of the cocktails before and after sonification confirm the first impression of better dispersion.

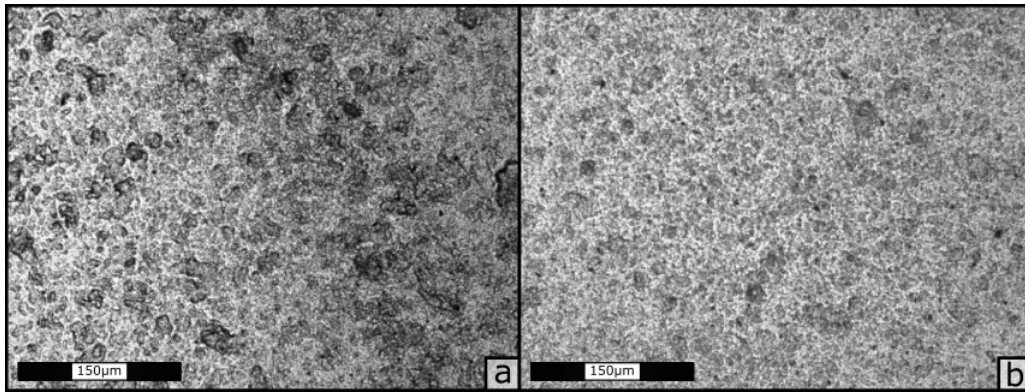


Figure 4.10: Microscopic image (20x magnification) of THF10; a(stirred), b(sonified)

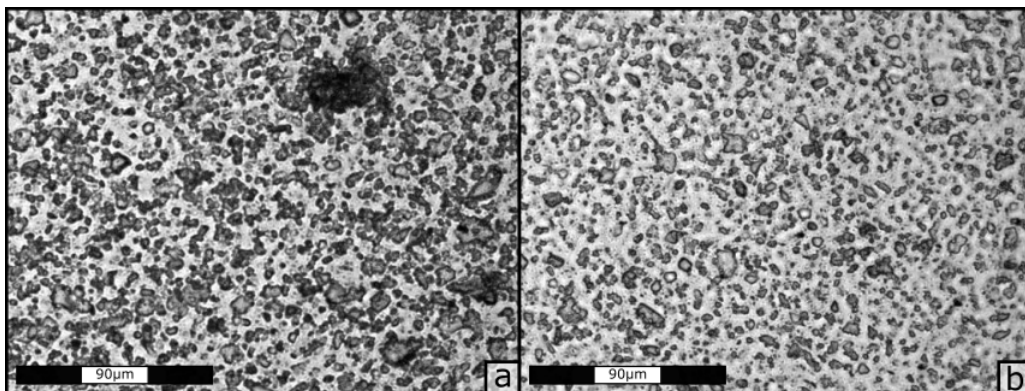


Figure 4.11: Microscopic image (40x magnification) of THF6; a(stirred), b(sonified)

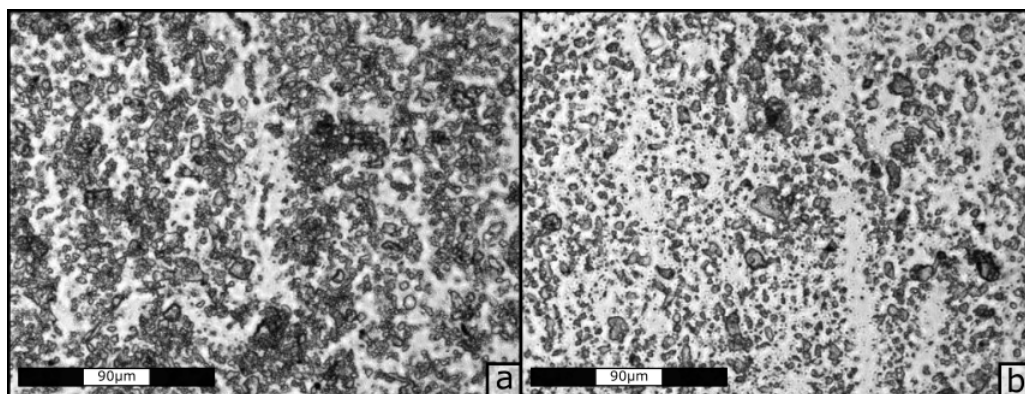


Figure 4.12: Microscopic image (40x magnification) of EtOH6; a(stirred), b(sonified)

Figure 4.10 demonstrates the difference in dispersion homogeneity before and after ultrasonic treatment. On the left side, dark stains mark dense particle agglomerates of the stirred cocktail, that are heavily reduced on the right side (sonified). In Figure 4.11 a close up on an agglomerate in THF6 of about 40 μm can be seen. Unfortunately, sonification can not prevent sedimentation completely. Precipitation of heavier particles will most likely occur inside the microdispensing system and further influence the printing behaviour. Sonification however will most likely decrease the chances of nozzle clogging.

4.3 Reproducibility evaluation of single spot and layer sensors

In this section produced oxygen and pH sensors are shown as a proof of concept for the successful small scale production. Selected photographs are provided as well as detailed results of profile measurements and sensor evaluation.

4.3.1 Reproducibility evaluation of oxygen sensors

The small spots are about 550 μm , whereas the square layers' edge length is in the range of 1200 μm . After drying, the layers show slight coffee rings, especially at the bigger layers. Since the single spots are smaller than the fiber diameter, differences in appearance should not affect the sensor operation, but agglomerations, height differences and concentration gradients within bigger sensor layers may lead to discrepancies in signal intensity and phase shift.

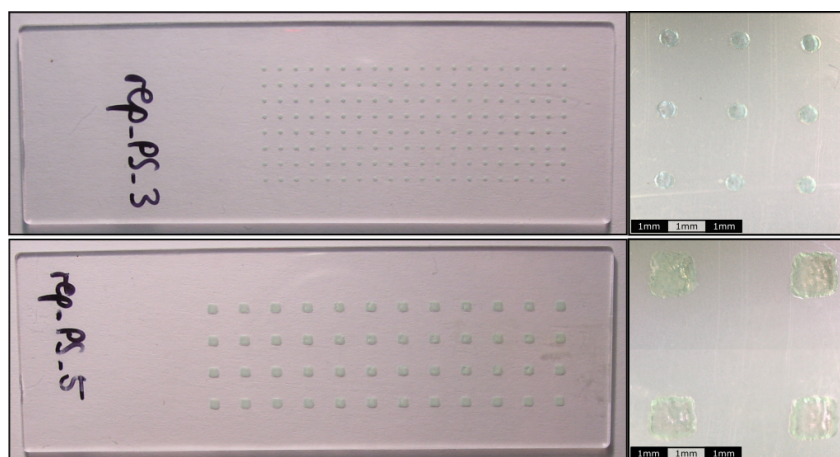


Figure 4.13: Pictures of finished oxygen sensor slides (3 layers each)

Profile measurement were performed for single spot and 3x3 matrix layer sensors with 1 and 3 printing passes each. For every variant five sensors were randomly chosen for profile evaluation.

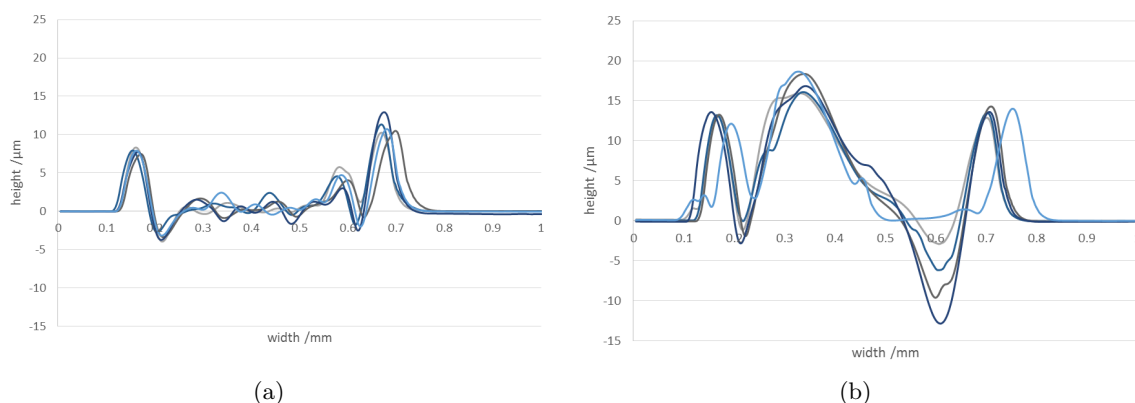


Figure 4.14: Profile measurements of single spot O_2 sensors; (a) 1 printing pass, (b) 3 printing passes

The single spot sensors both show heavy coffee ring formation as well as notch formation into the substrate. This is most likely originating in the solubility of polystyrene (substrate material) in used solvents. The sensor that was printed only once is almost at level with the substrate between the coffee ring elevations. The threefoldly printed sensor has a significant increase in bulk height to about 17 μm .

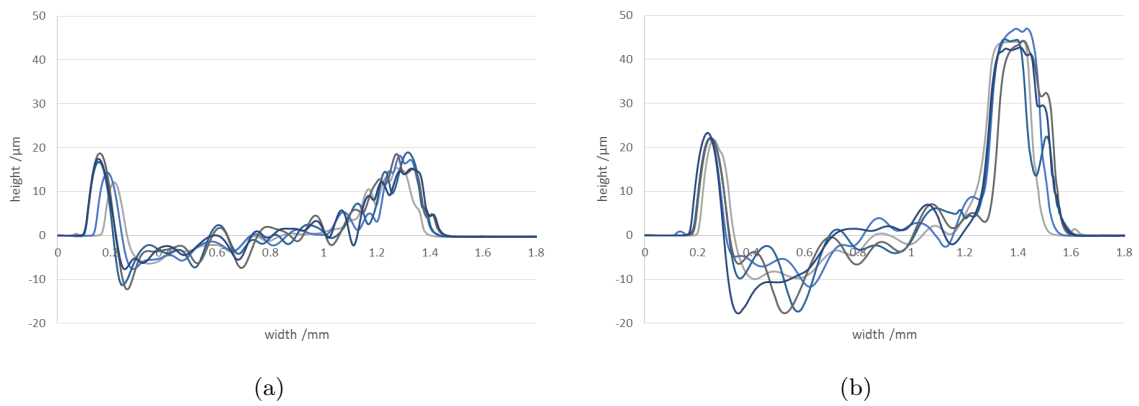


Figure 4.15: Profile measurements of 3x3 matrix layer O_2 sensors; (a) 1 printing pass, (b) 3 printing passes

The 3x3 matrix layers also have significant coffee ring formation. Contrary to the single spot sensors multiple printing steps does obviously not affect the center height of the sensor but increases the height of the elevated edges.

The following four diagrams contain evaluation data of every produced sensor. Measurements were done in water and Na_2SO_3 solution to simulate aerated and deaerated conditions.

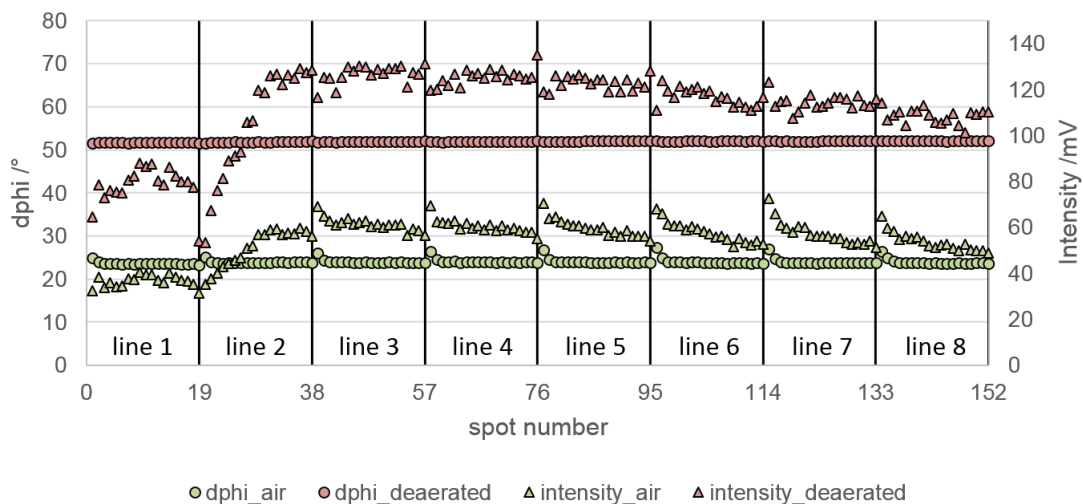


Figure 4.16: Phase shift and intensity of aerated and deaerated single spot oxygen sensors (1 printing pass)

In Figure 4.16 a very interesting phenomenon can be observed. The first printed line shows rather constant emission intensities that differ significantly from the values of the other 7 lines. There however, a decrease of intensity within the line can be seen. Given the signal rise in line two, it seems, that the dispensing process has some kind of "warm up phase", where the system has a significantly differing dispensing behaviour. Further it is also clearly visible that the first two to three spots in every line have not only higher intensity, but also increased phase shifts when aerated. The experiment was double checked to ensure that there is no O_2 partial pressure gradient, so the higher phase shifts are most likely originating in the dispensing process.

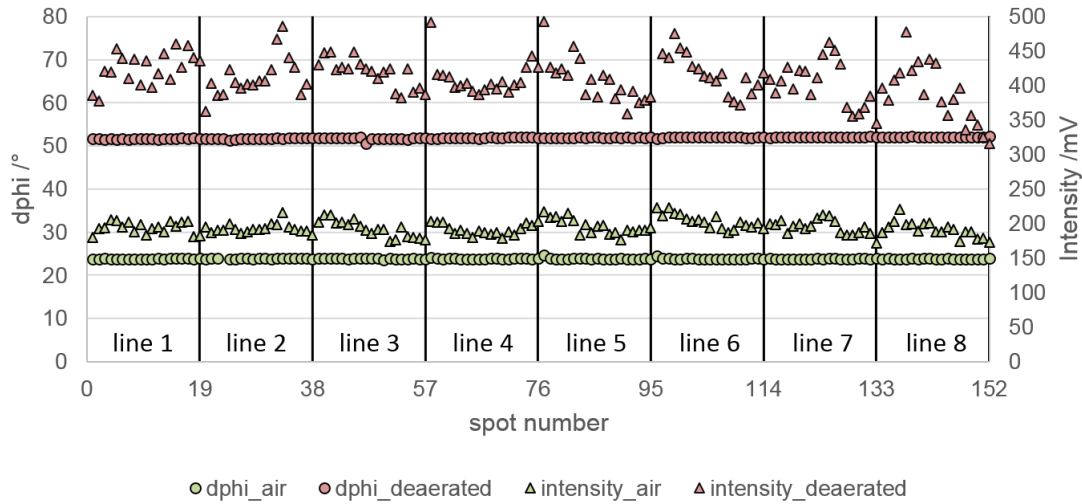


Figure 4.17: Phase shift and intensity of aerated and deaerated single spot oxygen sensors (3 printing passes)

Figure 4.17 shows the evaluation values of the single sensor slide that was printed three times. At first view it is apparent, that the signal intensities as well as the phase shifts do not have that characteristic drifts into one axis. Further, only line 5 and 6 show a distinguishable increase in phase shift when aerated. The rather constant evaluation values here indicate, that with the single layer, migration of dye into the polymer slide might be a problem. By increasing the sensor layer thickness and therefore raise the relative amount of sensor dye in the intended polymer matrix it seems, that the originating problem can be at least partly solved. A further advantage of this multilayer printing is the higher signal intensity of the small sensor spots.

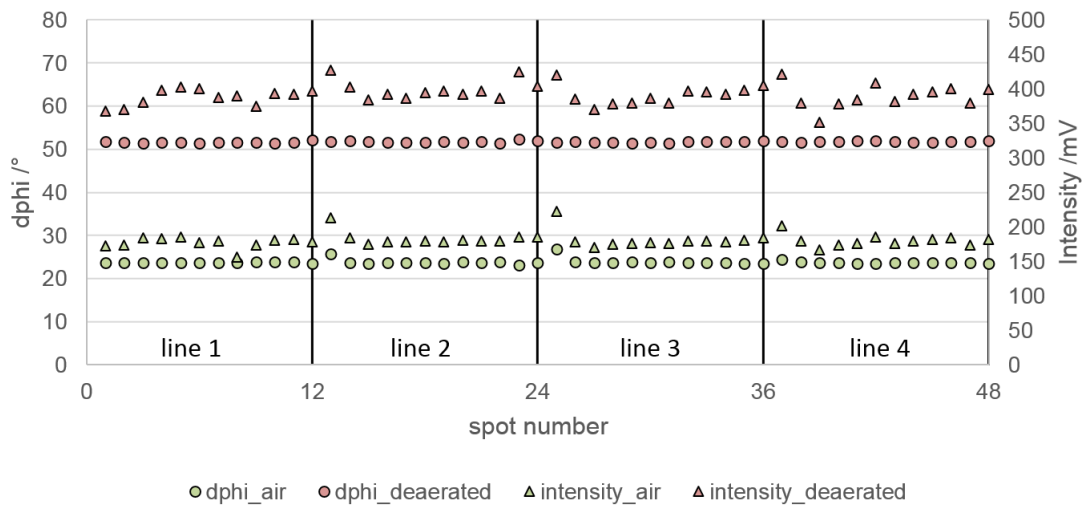


Figure 4.18: Phase shift and intensity of aerated and deaerated square layer oxygen sensors (1 printing pass)

The evaluation of the single layer square sensors is shown in Figure 4.18. Compared to the single spots, that were also printed only once, the intensities seem to be rather constant. The

first sensor in line 2, 3 and 4 however show the same behaviour regarding increased values in the first row. Considering the apparent optical inhomogeneity of the sensors, the signals are satisfying.

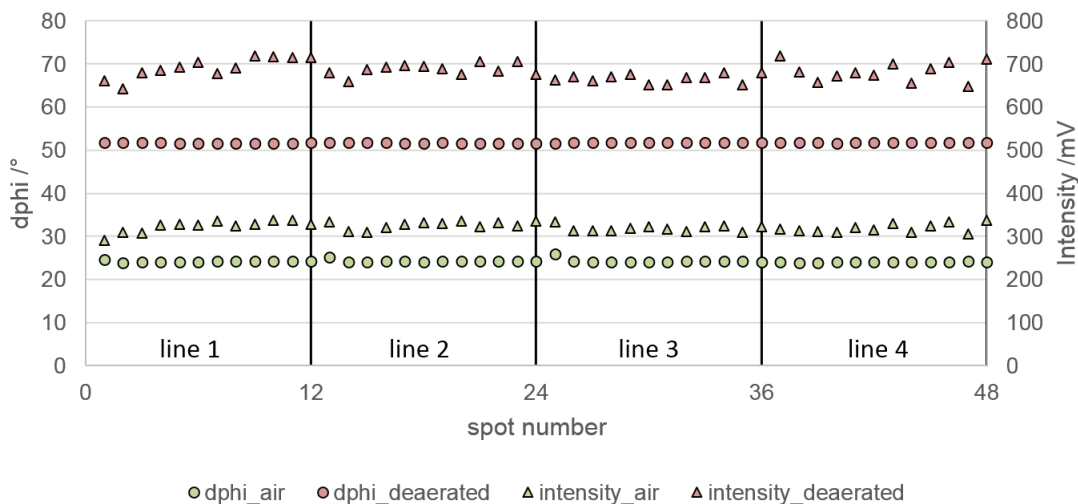


Figure 4.19: Phase shift and intensity of aerated and deaerated square layer oxygen sensors (3 printing passes)

Contrary to the single spots, there is no substantial improvement in signal consistency with the square layers that were printed three times (Figure 4.19). The first row from line 1 to 3 again has elevated air-values. Also, the deaerated intensity values in the range of 700 mV is far from three times of it's single printed counterpart (about 400 mV). As seen in Figure 4.13, the sensors have clearly visible coffee rings. This is most likely the cause of the low signal increase from 1 to 3 layers, since the sensor material obviously tends to accumulate on the edge of the layer.

The most reliable and reproducible method for sensor printing without intermediate cleaning steps may be the multilayer single spot. Given a readout system accurate enough the intensities are satisfying and the phase shifts are near to constant throughout a printing round of up to 150 sensors. Single layer spots are definitely not recommended in this particular case, since obviously there are inhomogenities for the produced layers. For larger sensors multiple layers do not pose a substantial improvement, at least when coffee ring formation is involved. Considering the evaluated experiments however, the respective single layer sensors seem to have adequate emission intensities. For later printings for each line 2 or 3 "sacrifice sensors" offside the substrate may be advised to get more stable results.

		aerated	deaerated
single spot 1x	phase shift /°	24.00±0.61	51.95±0.14
	intensity /mV	54.8±8.8	112.3±17.3
single spots 3x	phase shift /°	23.84±0.11	51.87±0.20
	intensity /mV	194.4±10.5	411.2±32.9
square layer 1x	phase shift /°	23.81±0.55	51.72±0.20
	intensity /mV	180.4±10.1	391.9±14.8
single spots 3x	phase shift /°	24.18±0.32	51.72±0.07
	intensity /mV	321.7±10.6	682.1±20.3

Table 4.9: Oxygen sensor evaluation; overview on intensity and phase shift mean values and standard deviation

Table 4.9 shows the results of all four oxygen slides as mean values and standard deviation of phase shifts and intensities. Deaerated phase shift signals are within a range of $\pm 0.07^\circ$ and $\pm 0.20^\circ$. Regarding aerated conditions the signals of triple printed sensor are within a tighter range, than the single printed ones.

4.3.2 Reproducibility evaluation of pH sensors

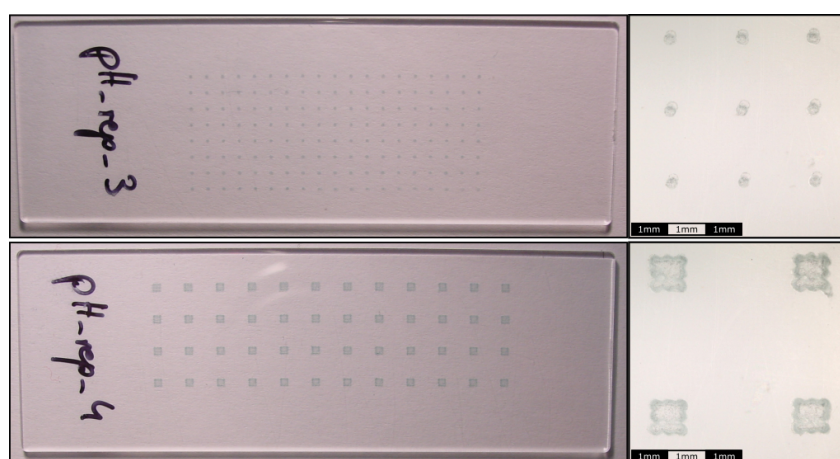


Figure 4.20: Pictures of finished pH sensor slides (3 layers each)

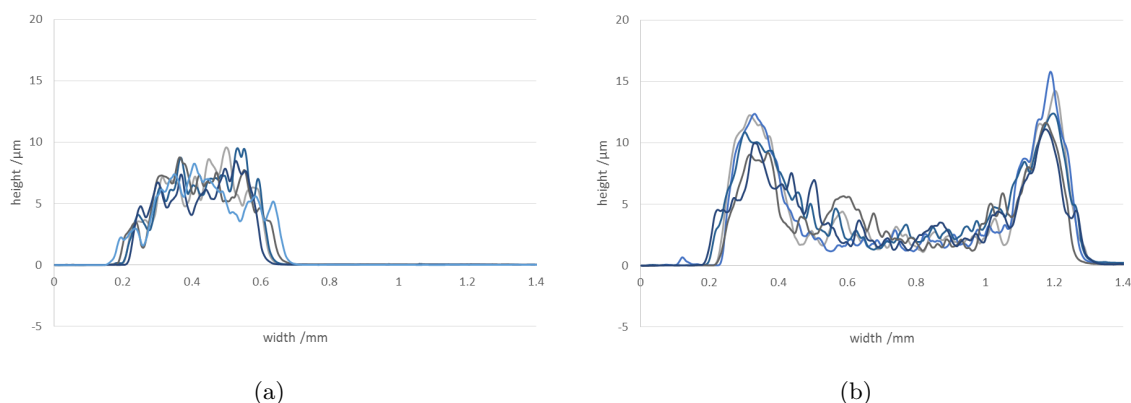


Figure 4.21: Profile measurements of produced pH sensors, three printing passes; (a) single spot, (b) 3x3 matrix layer

The range of sensor size is at 400 μm for the single spots and about 1000 μm for the 3x3 square layers. Whereas the larger layer have a rather consistent appearance throughout the slide, the single spots have visible disalignments during the different layers. Just from the first visible inspection significant differences in signals, especially at lower pH values (additional emission of the sensor dye) could be estimated. For the evaluation only the multiply printed sensors were considered, since the signal intensities of the single layer sensors were too low for adequate analysis. Contrary to the oxygen counterparts, these sensors show no notch formation and coffee rings are only observable at the 3x3 layers.

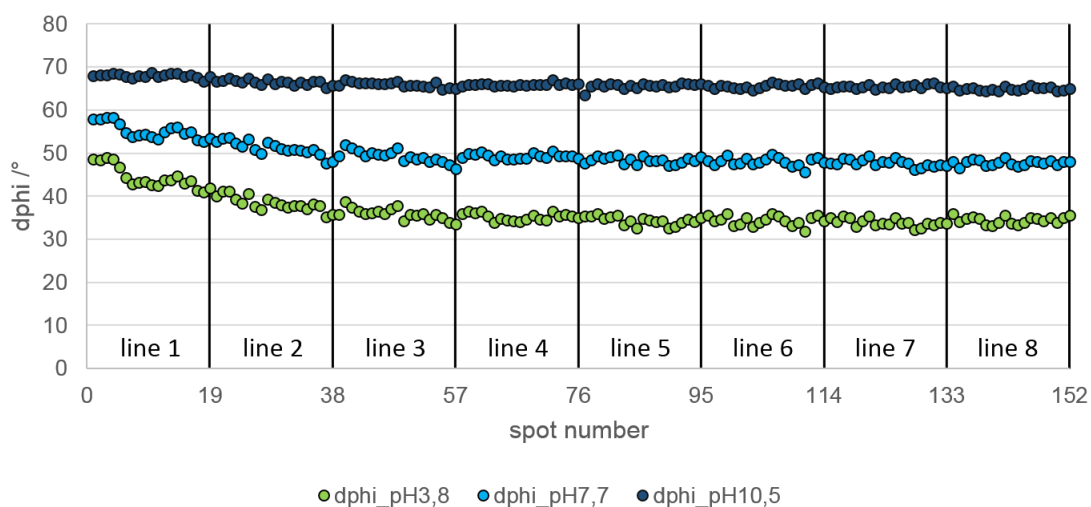


Figure 4.22: Phase shift of single spot sensors in different buffers (3 printing passes)

As seen in Figure 4.22, a similar behaviour in sensor printing is occurring for the pH sensors as for the oxygen sensors. Here again, a double check of the measurement setup was done to ensure that there is no pH gradient throughout the basin. Given the observation, that the phase shift signal of the deprotonated sensor is rather constant throughout the whole dispensing process, it seems that the ratio between reference dye and indicator dye drifts from less indicator in line 1

to more in line 4. From there on, the signal split stays rather constant, even though it is not as reproducible as with the oxygen sensors.

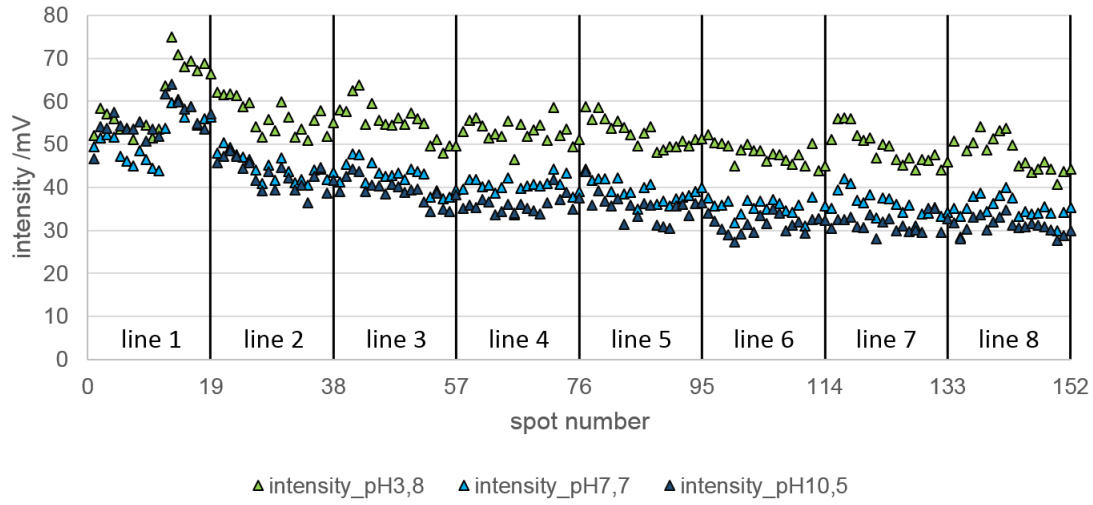


Figure 4.23: Intensity of single spot sensors in different buffers (3 printing passes)

Since the DLR system of the pH sensor is based on the emission of a sensor dye in addition to the reference dye, the intensity curves should look similar to the phase shift evaluation but inverted. This can be observed at the protonated sensor, although there is a drift, lower values in the first line and rather irreproducible values. At pH 7.7 and 10.5 on the other hand the intensities are not significantly different from each other. Considering the relatively large deviation in reference intensity (at pH 10.5 the signal is coming solely from Egyptian Blue) it is surprising, that the phase shift evaluations are rather acceptable.

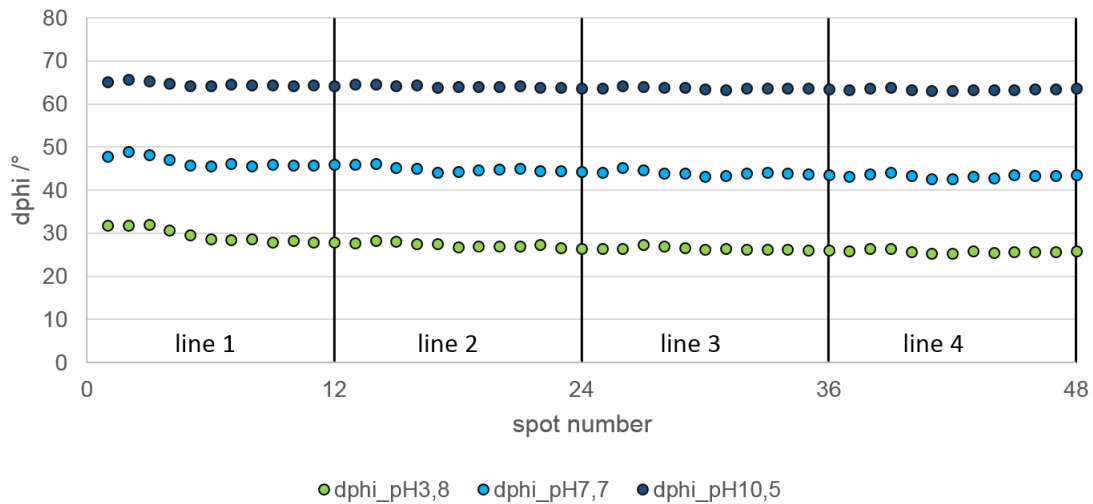


Figure 4.24: Phase shift of square layer sensors in different buffers (3 printing passes)

Compared to the single spots, the square layer sensor evaluation (Figure 4.24) delivers significantly better results. The phase shift of the protonated sensor drops from 32° to 27°

throughout the dispensing process, whereas the deprotonated sensor stays in a range between 63° and 66°.

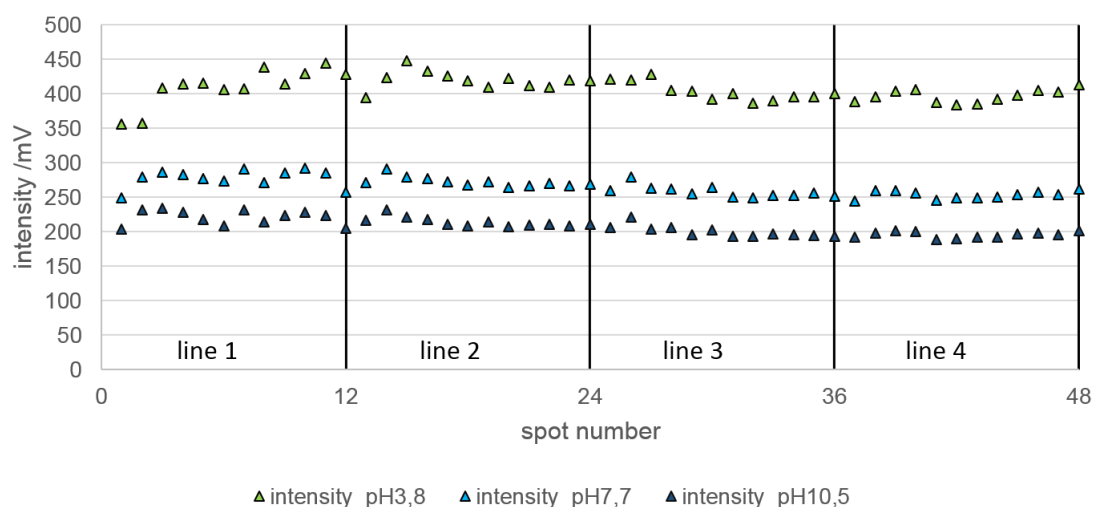


Figure 4.25: Intensity of square layer sensors in different buffers (3 printing passes)

In Figure 4.25 there is a significant split between intensity signals at different pH values observable. The deprotonated signal marks the low end of about 200 to 250 mV, going up to 400 mV at the protonated sensor. With a few exceptions, the emission intensities also remain rather constant from line 2.

		pH 3.8	pH 7.7	pH 10.5
single spots 3x	dphi /°	36.37±3.56	49.59±2.62	65.97±0.97
	intensity /mV	52.6±6.2	40.5±6.0	37.8±8.1
square layers 3x	dphi /°	27.26±1.66	44.69±1.42	63.98±0.57
	intensity /mV	407.6±18.7	265.3±13.2	207.77±12.7

Table 4.10: pH sensor evaluation; overview on intensity and phase shift mean values and standard deviation

In Table 4.10 a statistical evaluation of the single spot and layer sensors is given. Due to the drift through line 1 and 2 the phase shift values of the single spots show high standard deviations of 3.56° in acidic condition and 2.62° near the pK_a . Also the emission intensities vary heavily with the ranges even overlapping. The reproducibility obviously is a lot better with the square layers. Here, the highest deviation is at 1.66° for the acidic phase shift and also the intensity range is narrower speaking in relative terms.

Overall a few important observations could be made regarding pH sensor printing. Probably due to the sedimentation throughout the printing, a ratio drift can be perceived from beginning to end in favor of the sensor dye with ongoing dispensing time. Further, the inhomogeneity in phase shifts definitely makes distinct calibration for every single produced sensor necessary. This means, for every single sensor, at least a 2-point calibration has to be done after manufacturing.

Besides the flaws, it was a positive surprise to see the possibility of printing 152 sensors in one batch without the dispenser clogging.

4.4 Multilayer pH sensors

This section covers the evaluation of produced multilayer pH sensors. By assuming that the reference layers have rather comparable emission, the phase shift development of the sensor system is examined at increasing indicator amounts. With dispensing of multiple passes of indicator layer not only its emission intensity increases but also the spot diameter from about 250 μm to 50 μm (see Figure 4.26)

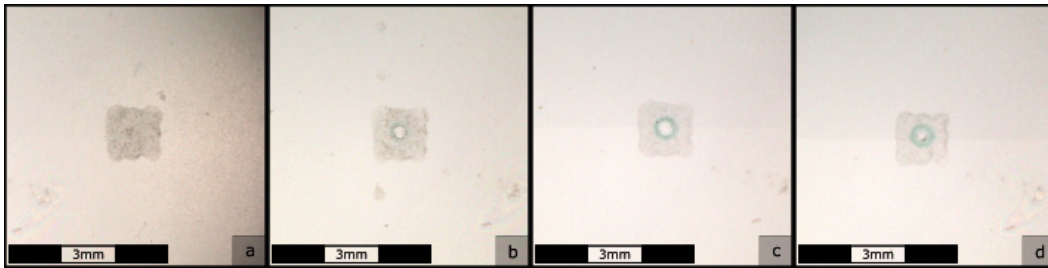


Figure 4.26: pH layer sensors with different numbers of indicator layer printing passes: a(0), b(6), c(14), d(22)

For the measurement the coffee ring should not interfere too strong due to the higher diameter of the piccolo₂ than the sensor spot. The calibration at pH 10.5 was expected to show constant values over the whole experiment. However, this was not the case, as there was a significant drift downwards in phase shift especially at the first few spottings.

layers	0	2	4	6	8	10	12	14	16	18	20	22
dphi _{pH3.8}	62.3	54.9	48.6	43.3	40.9	36.5	33.3	32.2	29.0	29.2	27.8	25.4
dphi _{pH7.7}	63.0	57.3	53.7	52.7	50.3	48.8	48.5	48.5	47.6	48.0	47.7	45.1
dphi _{pH10.5}	61.1	56.7	54.6	54.8	53.9	53.4	53.0	52.6	52.1	52.5	51.9	50.5

Table 4.11: Phase shift calibration values of pH layer sensors from 0 to 22 printing passes

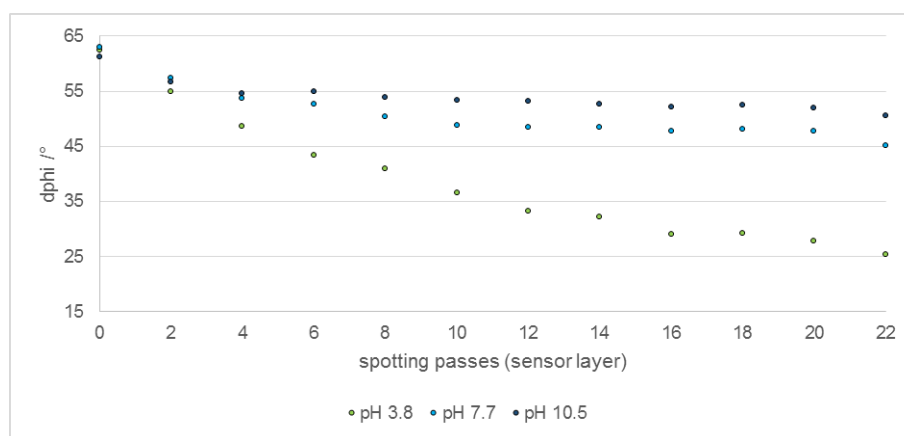


Figure 4.27: Calibration of produced pH layer sensors

The first set of calibration values demonstrates the phase shift signals of the sole Egyptian Blue layer at three different pH values. As expected these signals do not differ heavily, since no indicator dye is involved. With two pH sensitive layer printed the phase shifts decrease significantly without immense increase in signal split between acidic and basic conditions. The explanation for these effects is most likely sensor dye migration into the polymer substrate. This material exchange is enabled due to the use of toluene for the indicator solution and the solubility of polystyrene in it. This molecule exchange into the proton-impermeable matrix would lead to permanently protonated and luminescent sensor dye. Such sustained fluorescence is then interrupting with the reference signal in basic conditions and decrease the actual intensity range of the remaining pH sensitive part of the sensor dye. As the deprotonated phase shift signal is persistently decreasing with higher spotting passes, it can be assumed that the dye migration effect gets heavier with increasing printing numbers. The signal split however increases from 1.8° at 2 layers to 25.1° at 22 layers. Therefore this printing method with multiple layers can be considered an interesting way to rapidly produce multi-dye sensors with a large range regarding reference to sensor dye intensity.

4.5 Influence of spot distance on layer profile

Four sets of 4x4 layers (1 to 15 passes) were produced using the same cocktail, substrate and spotting parameters except spot distance. With a spot size around $300\ \mu\text{m}$, the distance was varied from $260\ \mu\text{m}$ to $320\ \mu\text{m}$ and the profile was then determined of each single layer.

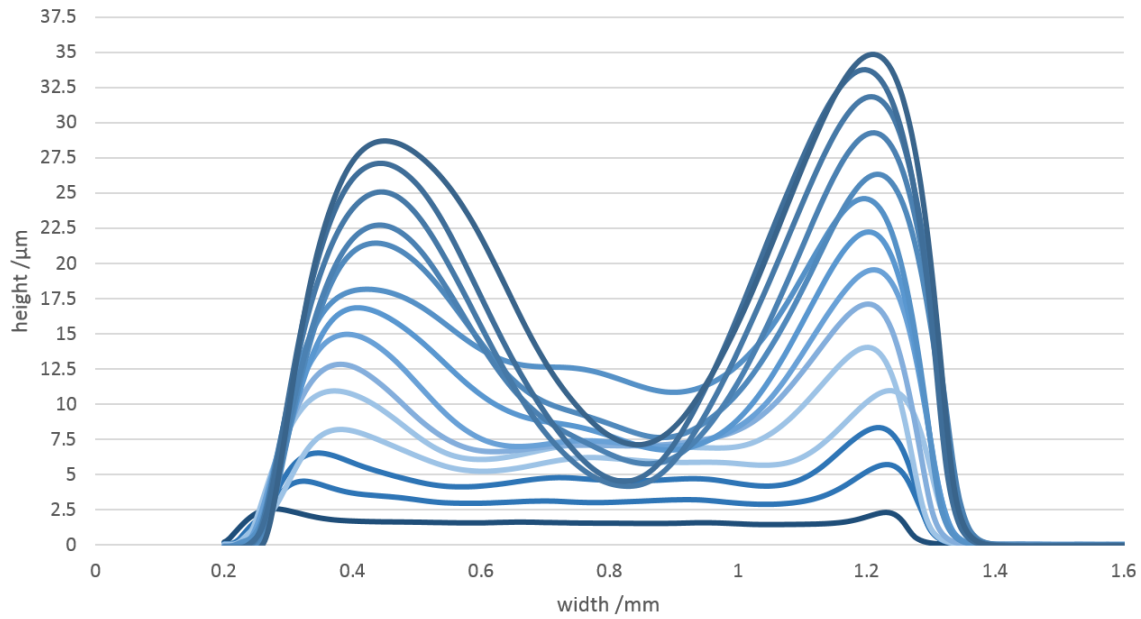


Figure 4.28: Layer profiles of 4x4 PS intermediate layers, 260 μm spot distance

It seems apparent in Figure 4.28 that there is a very heavy coffee ring formation of the layer above the 10th pass. It is assumed that the single spots were printed too narrowly to each other.

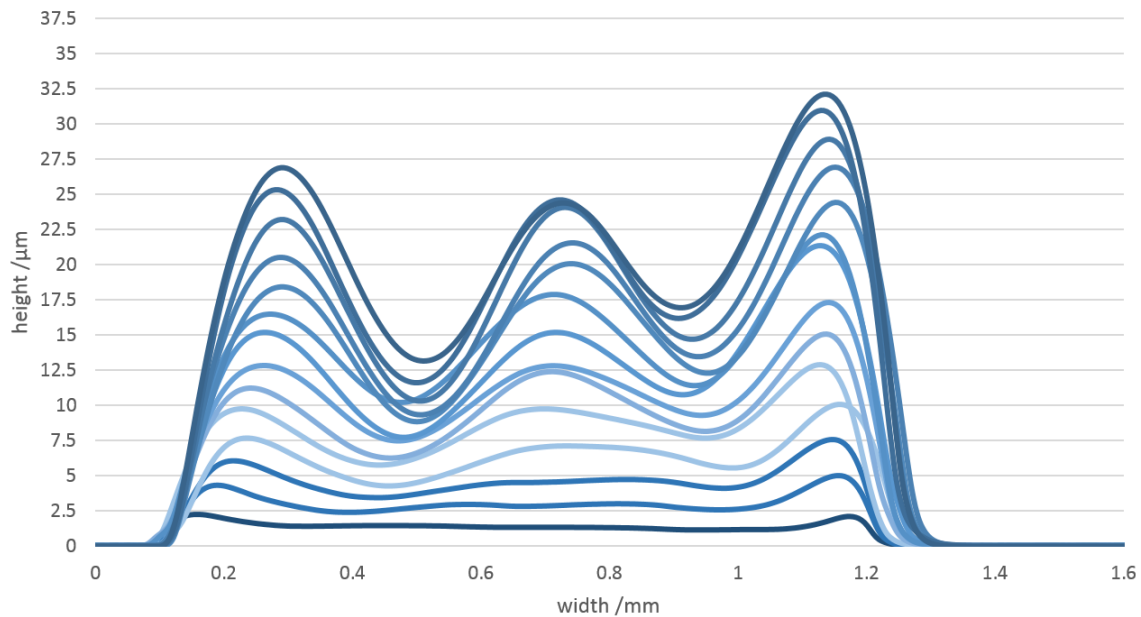


Figure 4.29: Layer profiles of 4x4 PS intermediate layers, 280 μm spot distance

Printing the layers with a slightly increased spot distance of 280 μm (seen in Figure 4.29) leads to an interesting drying behaviour regarding coffee ring formation. Instead of one dominating height minimum and two maxima on the outside, this printing method obviously leads to two

craters.

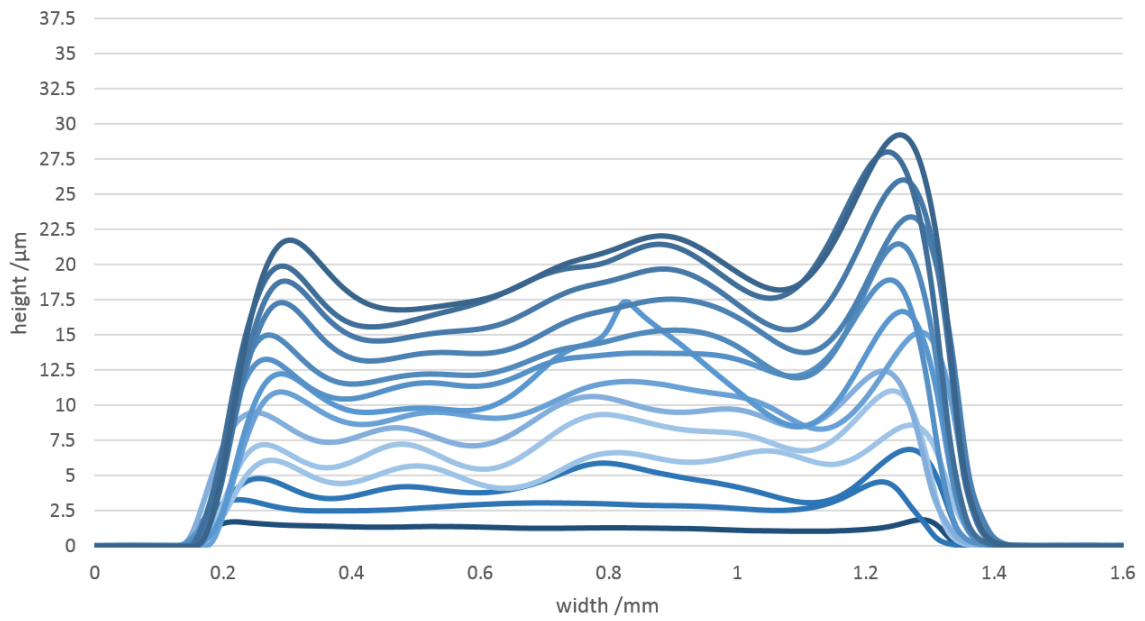


Figure 4.30: Layer profiles of 4x4 PS intermediate layers, 300 μm spot distance

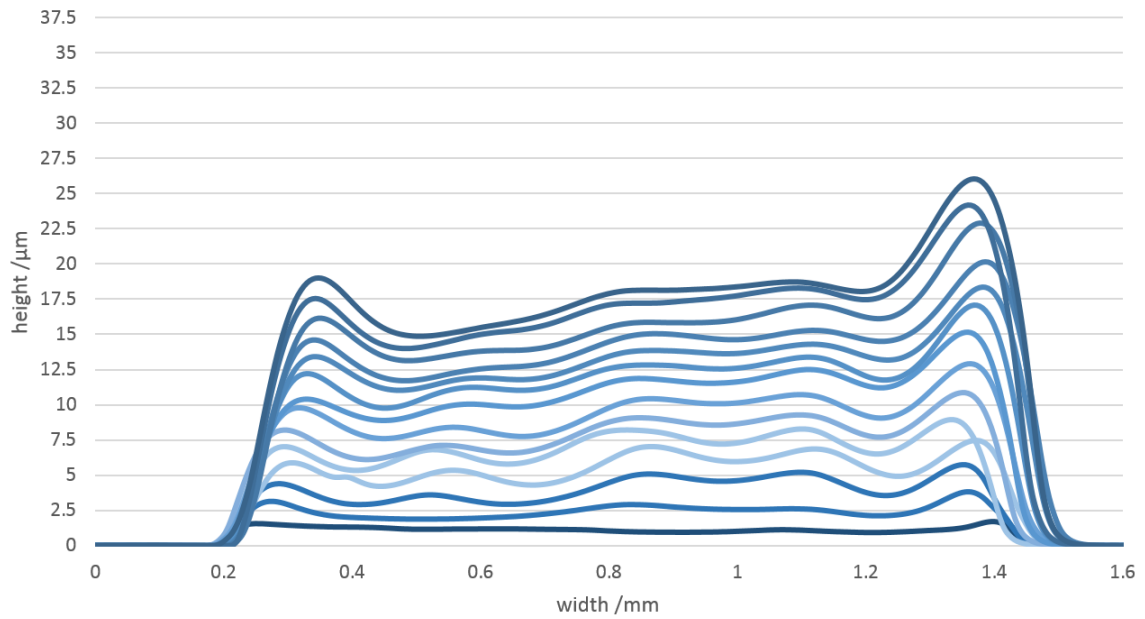


Figure 4.31: Layer profiles of 4x4 PS intermediate layers, 320 μm spot distance

As seen in Figures 4.30 and 4.31, further increasing of the spot distance improves the layer profile immensely. Despite the roughness, that is present especially around 5 μm layer height, the intermediate layers produced with 320 μm spot distance were used for migration investigation.

Table 4.12 shows the maximum and (inner) minimum height values in μm .

passes	PMMA260		PMMA280		PMMA300		PMMA320	
	high	low	high	low	high	low	high	low
1	2.30	1.55	1.97	1.33	1.55	1.28	1.43	0.97
2	5.44	3.03	4.84	2.40	4.41	2.50	3.80	1.87
3	8.10	4.13	7.27	3.46	6.78	3.39	5.70	2.94
4	10.85	5.23	9.96	4.26	8.47	4.13	6.72	4.23
5	13.76	6.04	12.86	5.77	11.00	5.60	8.89	5.35
6	16.97	6.62	14.79	6.32	12.69	7.37	10.74	6.15
7	19.31	7.00	17.25	7.70	15.61	8.63	12.90	7.62
8	21.99	6.85	21.27	7.75	16.90	8.48	15.02	8.88
9	24.44	10.85	22.04	10.39	18.90	10.44	16.88	9.76
10	26.25	7.83	24.32	9.30	21.62	11.50	18.16	11.04
11	29.04	5.25	26.77	9.37	23.33	13.17	20.05	11.72
12	31.79	4.52	28.34	10.38	25.77	14.56	22.56	13.14
13	33.47	4.55	30.90	11.61	28.41	15.58	24.08	13.98
14	34.56	7.13	32.04	13.19	29.12	16.81	25.61	14.86

Table 4.12: Minimum and maximum height values of intermediate layers printed with different spot distances

4.6 Evaluation of dye migration prevention through PS intermediate layers

3x3 matrix oxygen sensor layers were applied directly on the substrate as well as on polystyrene intermediate layers (prepared with 320 μm spot distance, see 4.5) The sensor that was applied directly to the polymer substrate demonstrates the maximum signal shift due to highest possible dye migration. Suitable numbers of intermediate layers are evaluated by determining the lowest height where no signal development is present with increasing printing passes anymore.

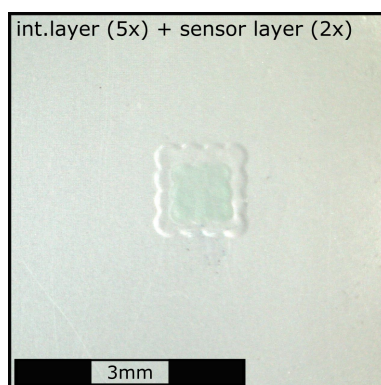


Figure 4.32: Image of a 3x3 oxygen sensor (PS) printed on a 4x4 intermediate layer (PS)

Evaluation of the oxygenated sensor showed that without intermediate layer the phase shift (23.6°) aberrates more than 5% from the original value in polystyrene alone (22.1°). For the

determination of height influence in migration effect the phase shift was applied versus the height minimum of the layer.

layer height / μm	0	0.97	1.87	2.94	4.23	5.35
dphi / $^\circ$	23.56	23.27	22.34	22.14	22.11	22.11

Table 4.13: Intermediate layer heights and their respective calibration values

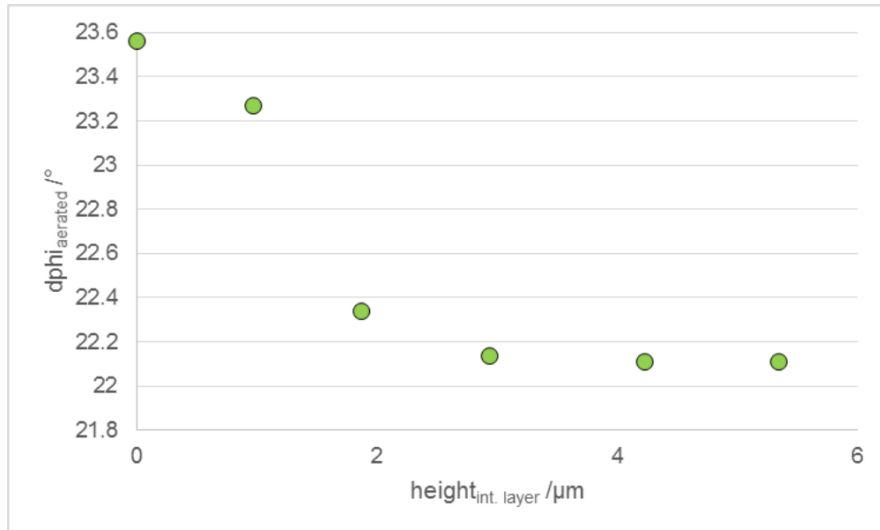


Figure 4.33: Phase shift of the oxygen sensor versus height of the intermediate layer

Figure 4.33 shows the evolution of the oxygen sensor phase shift at increasing intermediate layer heights. The curve flattens out at about 3 μm layer height. Further increasing does not have any significant impact on the phase shift value anymore. Therefore it can be said that for this cocktail and parameter setup 4 μm intermediate layer height (4 printing repetitions) is enough to prevent any unwanted sensor dye migration into the polymer slide.

5 Conclusion and Outlook

After successful installment of the microdispensing device to a CNC machine and finished coding for all necessary software parts high effort was carried out to find suitable cocktail compositions for different sensor matrices such as polystyrene and D4 hydrogel. Due to the high amount of different parameters the multidimensional aspect of this search represented the biggest challenge. After gathering enough data to provide sufficient cocktail compositions and fitting parameters, a few examples have been shown on the possibilities of microdispensing technology for sensor printing. A few aspect of the technology make it an interesting tool for small scale sensor application and development:

- easily adaptable for different matrix materials
- wide range of usable solvent(mixtures) and viscosities
- possibility of employing larger particles due to high viscosity sedimentation prevention
- spot sizes down to 250 μm
- exact sensor placement with 1 μm movement step

At this development stage, the microdispenser presented in this thesis is able to apply oxygen and pH sensors as single spots or layers of adjustable sizes. It was shown that manufacturing of 150 single sensor spots (pH and oxygen) as well as 50 layer sensors can be carried out in one single production step. Further there is a rather satisfying reproducibility in oxygen sensor production throughout the whole process. Regarding pH sensors there is still room for improvement especially considering reference material precipitation.

Oxygen sensors

The production of about 300 single spot and 100 layer O₂ sensors was carried out as well as 800 measurements for overview characterization. The investigations showed that multiple printing steps onto a single location provides not only higher signal intensities but also better signal reproducibility. It was also shown that for polymer substrates it may be interesting to prepare intermediate layers out of sole matrix material to prevent dye migration into the substrate and therefore calibration shifts. These investigations also led to valuable information about the height development of polymer layers if printed on top of each other. This knowledge can be used for better layer height management in the future.

pH sensors

Prior to any pH sensor printing the sedimentation behaviour of Egyptian Blue was examined and a preparation method was stated for best possible particle dispersion. Whereas high dispersion viscosities were chosen to diminish sedimentation effects, sensor application results showed that it is still an issue. Besides the lacking reproducibility in sensor preparation, it is

possible to prepare hundreds of pH sensors in a single batch without clogging at sizes down to 250 μm . The ability of fast medium exchange and height control can make the system a practical alternative for other DLR systems and absorption based sensors with multiple layers for example.

Possible future developments and applications

Alongside the work on this thesis also a few prototype applications have already been carried out. In cooperation with University College London pH sensor spots with sizes of about 350 μm were implemented into a custom made microfluidic chip.



Figure 5.1: Polymer microfluidic chip with 40 integrated pH sensor spots of about 350 μm each

Another project was carried out where sets of ethyl cellulose indicator layers for multilayer CO_2 sensors with different layer heights were prepared for sensor optimization purposes.

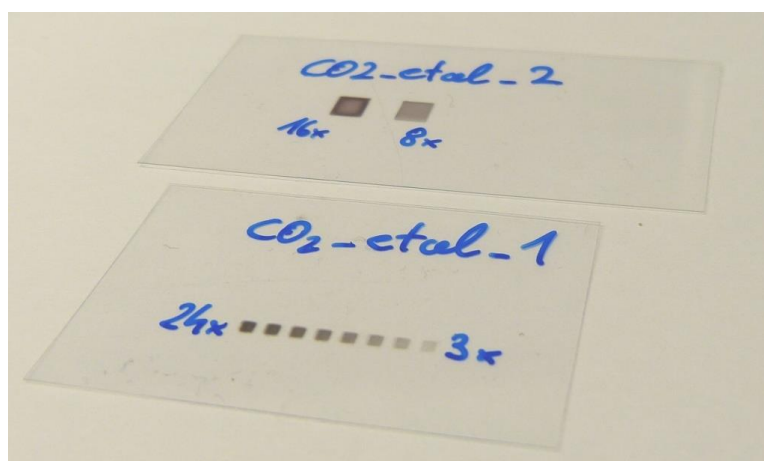


Figure 5.2: CO_2 indicator layers printed with different layer heights printed on polymer foil

Besides the fully functional infrastructure for oxygen and pH sensor printing the method has potential for a wide range of additional applications. Depending on future use frequency one or more of the following improvements can be considered:

- device control on a single PC
- additional sensors and sensor matrices
- provision of a comprehensive cocktail-parameter catalogue
- optical positioning system

6 References

- (1) Liebsch, G.; Klimant, I.; Krause, C.; Wolfbeis, O. S. *Analytical Chemistry* **Sept. 1, 2001**, *73*, 4354–4363.
- (2) Koren, K., *Optical oxygen sensors - indicators and materials: synthesis and applications*, 2012.
- (3) Waich, K.; Borisov, S.; Mayr, T.; Klimant, I. *Sensors and Actuators B: Chemical* **May 20, 2009**, *139*, 132–138.
- (4) Pasic, A.; Koehler, H.; Klimant, I.; Schaupp, L. *Sensors and Actuators B: Chemical* **Mar. 8, 2007**, *122*, 60–68.
- (5) Mayr, T.; Klimant, I.; Wolfbeis, O. S.; Werner, T. *Analytica Chimica Acta* **June 26, 2002**, *462*, 1–10.
- (6) Chang, Y.-H.; Tseng, S.-R.; Chen, C.-Y.; Meng, H.-F.; Chen, E.-C.; Horng, S.-F.; Hsu, C.-S. *Organic Electronics* **Aug. 2009**, *10*, 741–746.
- (7) Trommer, K.; Petzold, C.; Morgenstern, B.; Trommer, K.; Petzold, C.; Morgenstern, B. *Journal of Applied Chemistry, Journal of Applied Chemistry* **Aug. 17, 2014**, *2014*, *2014*, e307274.
- (8) Pierre, A.; Sadeghi, M.; Payne, M. M.; Facchetti, A.; Anthony, J. E.; Arias, A. C. *Advanced Materials* **Aug. 1, 2014**, *26*, 5722–5727.
- (9) Abel, T.; Ungerböck, B.; Klimant, I.; Mayr, T. *Chemistry Central Journal* **Oct. 26, 2012**, *6*, 124.
- (10) Wencel, D.; Abel, T.; McDonagh, C. *Analytical Chemistry* **Jan. 7, 2014**, *86*, 15–29.
- (11) Ehgartner, J.; Sulzer, P.; Burger, T.; Kasjanow, A.; Bouwes, D.; Krühne, U.; Klimant, I.; Mayr, T. *Sensors and Actuators B: Chemical* **June 2, 2016**, *228*, 748–757.
- (12) Kumar, P.; Shin, P. K.; Ochiai, S. In *2012 19th International Workshop on Active-Matrix Flatpanel Displays and Devices (AM-FPD)*, 2012 19th International Workshop on Active-Matrix Flatpanel Displays and Devices (AM-FPD), July 2012, pp 293–296.
- (13) Karthick, S. N.; Richard Prabhu Gnanakan, S.; Subramania, A.; Kim, H.-J. *Journal of Alloys and Compounds* **Jan. 21, 2010**, *489*, 674–677.
- (14) Seidel, S. M.; Jeschke, S.; Vettikuzha, P.; Wiemhofer, H.-D. *Chem. Commun.* **2015**, *51*, 12048–12051.
- (15) Zhuang, Y.; Yu, D.; Dai, F.; Niu, Z. *Microsystem Technologies* **Mar. 2016**, *22*, 639–643.
- (16) Chiang, C.-H.; Tseng, Z.-L.; Wu, C.-G. *Journal of Materials Chemistry A* **Sept. 9, 2014**, *2*, 15897–15903.
- (17) Mitzi, D. B.; Kosbar, L. L.; Murray, C. E.; Copel, M.; Afzali, A. *Nature* **Mar. 18, 2004**, *428*, 299–303.
- (18) Kadhim, I. H.; Hassan, H. A. *Journal of Materials Science: Materials in Electronics* **Jan. 14, 2016**, 1–7.

-
- (19) Wang, E.; Chow, K.-F.; Kwan, V.; Chin, T.; Wong, C.; Bocarsly, A. *Analytica Chimica Acta* **Oct. 24, 2003**, *495*, 45–50.
- (20) Brglez, P.; Holobar, A.; Pivec, A.; Kolar, M. *MATERIALI IN TEHNOLOGIJE* **Mar. 2014**, *48*, 181–188.
- (21) Krebs, F. C.; Jørgensen, M.; Norrman, K.; Hagemann, O.; Alstrup, J.; Nielsen, T. D.; Fyenbo, J.; Larsen, K.; Kristensen, J. *Solar Energy Materials and Solar Cells* **Apr. 2009**, *93*, 422–441.
- (22) Vasudivan, S.; Zhiping, W. In *Electronics Packaging Technology Conference (EPTC), 2010 12th*, Electronics Packaging Technology Conference (EPTC), 2010 12th, Dec. 2010, pp 89–93.
- (23) Mayr, T.; Abel, T.; Kraker, E.; Köstler, S.; Haase, A.; Konrad, C.; Tscherner, M.; Lamprecht, B. *Procedia Engineering* **2010**, *5*, 1005–1008.
- (24) Subramanian, V.; Cen, J.; Vornbrock, A. d. l. F.; Grau, G.; Kang, H.; Kitsomboonloha, R.; Soltman, D.; Tseng, H. Y. *Proceedings of the IEEE* **Apr. 2015**, *103*, 567–582.
- (25) De Gans, B.-J.; Duineveld, P. C.; Schubert, U. S. *Advanced Materials* **Feb. 3, 2004**, *16*, 203–213.
- (26) Li, J.; Rossignol, F.; Macdonald, J. *Lab on a Chip* **June 1, 2015**, *15*, 2538–2558.
- (27) Yorov, K. E.; Grigorieva, A. V.; Sidorov, A. V.; Polyakov, A. Y.; Sukhorukova, I. V.; Shtansky, D. V.; Grünert, W.; Goodilin, E. A. *RSC Advances* **Feb. 5, 2016**, *6*, 15535–15540.
- (28) Maejima, K.; Tomikawa, S.; Suzuki, K.; Citterio, D. *RSC Advances* **May 28, 2013**, *3*, 9258–9263.
- (29) Hoera, C.; Skadell, M. M.; Pfeiffer, S. A.; Pahl, M.; Shu, Z.; Beckert, E.; Belder, D. *Sensors and Actuators B: Chemical* **Mar. 31, 2016**, *225*, 42–49.
- (30) Poehler, E.; Herzog, C.; Pfeiffer, S. A.; Lotter, C.; Peretzki, A. J.; Aigner, D.; Mayr, T.; Beckert, E.; Nagl, S. *Procedia Engineering* **2015**, *120*, 175–179.
- (31) Binder, S.; Glatthaar, M.; Rädlein, E. *Aerosol Science and Technology* **Sept. 2, 2014**, *48*, 924–929.
- (32) Jabari, E.; Toyserkani, E. *Materials Letters* **July 1, 2016**, *174*, 40–43.
- (33) Tait, J. G.; Witkowska, E.; Hirade, M.; Ke, T.-H.; Malinowski, P. E.; Steudel, S.; Adachi, C.; Heremans, P. *Organic Electronics* **July 2015**, *22*, 40–43.
- (34) Wu, X.; Chen, Z.; Zhou, T.; Shao, S.; Xie, M.; Song, M.; Cui, Z. *RSC Advances* **Feb. 20, 2015**, *5*, 20924–20930.
- (35) Hood-Daniel, P.; Kelly, J. F., *Build Your Own CNC Machine*; Apress: Nov. 30, 2009; 240 pp.
- (36) Hans B. Kief; Helmut A. Roschiwal; Karsten Schwarz In *CNC-Handbuch 2015/2016*, Hans B. Kief, Karsten Schwarz, Helmut A. Roschiwal, Eds., 0 vols.; Carl Hanser Verlag GmbH & Co. KG: Jan. 15, 2015, pp 1–14.
- (37) Lakowicz, J. R., *Principles of fluorescence spectroscopy*, 2.; Kluwer Acad., Plenum Publ: New York, NY [u.a.], 1999.
- (38) Valeur, B., *Molecular fluorescence: principles and applications*; Wiley-VCH: Weinheim [u.a.], 2002.

- (39) Strobl, M.; Rappitsch, T.; Borisov, S. M.; Mayr, T.; Klimant, I. *Analyst* **Oct. 12, 2015**, *140*, 7150–7153.
- (40) Klimant, I.; Huber, C.; Liebsch, G.; Neurauder, G.; Stangelmayer, A.; Wolfbeis, O. S. In, Valeur, B., Brochon, J.-C., Eds.; Springer Berlin Heidelberg: Berlin, Heidelberg, 2001, pp 257–274.
- (41) Boniello, C.; Mayr, T.; Bolivar, J. M.; Nidetzky, B. *BMC Biotechnology* **2012**, *12*, 11.
- (42) Begemann, J.; Spiess, A. C. *Biotechnology Journal* **Sept. 1, 2015**, *10*, 1822–1829.
- (43) Martínez Ferreras, F.; Wolfbeis, O. S.; Gorris, H. H. *Analytica Chimica Acta* **June 4, 2012**, *729*, 62–66.
- (44) Borisov, S. M.; Neurauder, G.; Schroeder, C.; Klimant, I.; Wolfbeis, O. S. *Applied Spectroscopy* **Oct. 1, 2006**, *60*, 1167–1173.

7 List of Figures

2.1	Schematic presentation of a knife coating process	2
2.2	Working principle of spray coating with and without mask	3
2.3	Layer application through spin coating	4
2.4	Schematic presentation of a screen printing process	5
2.5	Droplet ejection through mechanical piezo contraction	6
2.6	Layer application by aerosol jet printing	7
2.7	Jablonski diagram	9
2.8	Luminescence quenching through complex foramation	10
2.9	Dynamic quenching mechanism	11
2.10	Photoinduced electron transfer	12
2.11	Emission and shifted excitation signal at phase fluorimetry	12
2.12	Phase shift measurement through a single fiber device	13
2.13	Signal development of a DLR system at low and high sensor emission	14
3.1	Illustration of the CNC setup	18
3.2	Illustration of the completed system	19
3.3	Photograph of the completed system	19
3.4	Spotting variables illustrated	20
3.5	Graphic interface of LinuxCNC showing a 3x3 square pattern	22
3.6	Graphic LabView interface: MDU remote control	23
3.7	Schematic picture of the working principle of a microdispensing device	24
3.8	Diagram of a single dispensing step; tappet lift vs. time	24
3.9	Schematic presentation of different tappet sizes	25
3.10	Different methods of sensor printing	26
3.11	Scheme of prepared sensor slides, 8x19 for small spots and 4x12 for square layers	28
3.12	Automated phase shift readout system	30
3.13	pH layer sensor with different amounts of sensor dye	30
3.14	Schematic illustration of printed sensors with and without intermediate layers .	31
3.15	Sensor centered on an intermediate layer	32
4.1	PS.6.tol_lift_2: spots prepared with varying tappet lifts and minimum falling time; lift/falling time: a(23%/0.03 ms), b(26%/0.03 ms), c(29%/0.03 ms), d(32%/0.04 ms)	35
4.2	PS.6.tol_lift_3: spots prepared with varying tappet lifts and minimum falling time; lift/falling time: a(32%/0.04 ms), b(40%/0.04 ms), c(50%/0.05 ms), d(60%/0.06 ms)	35
4.3	PS.12.tol.80.chlor.20_fall_2: spots prepared with varying falling times; lift/- falling time: a(60%/0.40ms), b(60%/0.20ms), c(60%/0.10ms), d(60%/0.06ms) .	36
4.4	PS.15.EtOAc_fall_1: spots prepared with varying falling times; lift/falling time: a(50/0.40ms), b(50/0.20ms), c(50/0.10ms), d(50/0.05ms)	37

4.5	PS.6.tol_pressure_1: spots prepared with varying reservoir pressures; pressure: a(0.4bar), b(0.6bar), c(0.8bar), d(1.0bar)	38
4.6	PS.6.tol_pressure_2: spots prepared with varying reservoir pressures; pressure: a(0.4 bar), b(0.6 bar), c(0.8 bar), d(1.0 bar)	39
4.7	PS.12.tol.80.chlor.20_distance_1: spots prepared with varying substrate-nozzle distances; distance: a(15 mm), b(12 mm), c(3 mm), d(2 mm)	40
4.8	EB cocktail after 10 min stirring; from left: THF 6, THF 10, EtOH 6, EtOH 10	40
4.9	EB cocktail after 15 s sonification; from left: THF 6, THF 10, EtOH 6, EtOH 10	41
4.10	Microscopic image (20x magnification) of THF10; a(stirred), b(sonified) . .	41
4.11	Microscopic image (40x magnification) of THF6; a(stirred), b(sonified) . . .	41
4.12	Microscopic image (40x magnification) of EtOH6; a(stirred), b(sonified) . .	42
4.13	Pictures of finished oxygen sensor slides (3 layers each)	43
4.14	Profile measurements of single spot O ₂ sensors; (a) 1 printing pass, (b) 3 printing passes	43
4.15	Profile measurements of 3x3 matrix layer O ₂ sensors; (a) 1 printing pass, (b) 3 printing passes	44
4.16	Phase shift and intensity of aerated and deaerated single spot oxygen sensors (1 printing pass)	44
4.17	Phase shift and intensity of aerated and deaerated single spot oxygen sensors (3 printing passes)	45
4.18	Phase shift and intensity of aerated and deaerated square layer oxygen sensors (1 printing pass)	45
4.19	Phase shift and intensity of aerated and deaerated square layer oxygen sensors (3 printing passes)	46
4.20	Pictures of finished pH sensor slides (3 layers each)	47
4.21	Profile measurements of produced pH sensors, three printing passes; (a) single spot, (b) 3x3 matrix layer	48
4.22	Phase shift of single spot sensors in different buffers (3 printing passes)	48
4.23	Intensity of single spot sensors in different buffers (3 printing passes)	49
4.24	Phase shift of square layer sensors in different buffers (3 printing passes)	49
4.25	Intensity of square layer sensors in different buffers (3 printing passes)	50
4.26	pH layer sensors with different numbers of indicator layer printing passes: a(0), b(6), c(14), d(22)	51
4.27	Calibration of produced pH layer sensors	52
4.28	Layer profiles of 4x4 PS intermediate layers, 260 μm spot distance	53
4.29	Layer profiles of 4x4 PS intermediate layers, 280 μm spot distance	53
4.30	Layer profiles of 4x4 PS intermediate layers, 300 μm spot distance	54
4.31	Layer profiles of 4x4 PS intermediate layers, 320 μm spot distance	54
4.32	Image of a 3x3 oxygen sensor (PS) printed on a 4x4 intermediate layer (PS) . .	55
4.33	Phase shift of the oxygen sensor versus height of the intermediate layer	56
5.1	Polymer microfluidic chip with 40 integrated pH sensor spots of about 350 μm each	58
5.2	CO ₂ indicator layers printed with different layer heights printed on polymer foil	58

8 List of Tables

3.1	Sensor printer parts	16
3.2	Devices used for measurement and recording	16
3.3	Sonifier parts for particle dispensing	16
3.4	Solvents used	17
3.5	Polymers used	17
3.6	Sensor and reference dyes used	17
3.7	Programming variables for the G-code file	21
3.8	Crucial parameters for dispensing	25
3.9	Necessary parameter changes for unwanted spotting issues	26
3.10	Cocktails prepared for dispensing tests	27
3.11	Sonification parameters for Egyptian Blue dispersing	27
3.12	Cocktail compositions for the reproducibility tests	28
3.13	Dispensing parameters for the reproducibility tests	29
3.14	Buffer solutions for pH calibration	29
3.15	Cocktail compositions for the pH layer sensors	31
3.16	Dispensing parameters for the pH layer sensors	31
3.17	Cocktail compositions for printing intermediate PS layers	32
3.18	Dispensing parameters for printing intermediate layers	32
3.19	Cocktail compositions for printing oxygen sensors on PS intermediate layers	32
4.1	Lowest possible falling times	34
4.2	Dispensing parameters for PS.6.tol_lift_2 150805	34
4.3	Dispensing parameters for PS.6.tol_lift_3 150805	35
4.4	Dispensing parameters for PS.12.tol.80.chlor.20_fall_2 150810	36
4.5	Dispensing parameters for PS.15.EtOAc_fall_1 150817	37
4.6	Dispensing parameters for PS.6.tol_pressure_1 150805	38
4.7	Dispensing parameters for PS.6.tol_pressure_2 150805	38
4.8	Dispensing parameters for PS.12.tol.80.chlor.20_distance_1 150810	39
4.9	Oxygen sensor evaluation; overview on intensity and phase shift mean values and standard deviation	47
4.10	pH sensor evaluation; overview on intensity and phase shift mean values and standard deviation	50
4.11	Phase shift calibration values of pH layer sensors from 0 to 22 printing passes	51
4.12	Minimum and maximum height values of intermediate layers printed with different spot distances	55
4.13	Intermediate layer heights and their respective calibration values	56

9 Appendix

9.1 CNC control (G-code)

```
%
2 (for you to change)

#<correction_y>      = 15.0    (correction in x axis in mm)
#<correction_x>      = 15.0    (correction in y axis in mm)
7 #<correction_z>     = 0.0     (correction in z axis in mm)
#<squares_per_line>  = 3       (number of squares in y direction)
#<lines>             = 2       (number of lines)
#<square_length>     = 3       (number of spots per square edge)
#<dist_squares_y>    = 8       (distance of squares in line)
12 #<dist_squares_x>  = 4       (distance between lines)
#<spot_distance>     = 0.33    (distance between spots in square)
#<repeat_all>        = 1       (repeat all including cleaning process)
#<wait_all>          = 0       (waiting time between repetitions)

17 (try not to change those. if you do, be careful! If you have questions ask Fipsotron)

#<repeat_count>=1
#<move_speed>=4000
22 #<wait_pass> = 0.005 (wait between passes)
#<wait_trigger> = 0.02 (wait trigger)
#<repeat_clean> = 8 (cleaning steps)
#<wait_clean> = 0.03
#<repeat_all> = 1
27 #<wait_all> = 0

(program starts here)

0109 if [#<correction_y> GE 0]
32 0108 if [#<correction_x> GE 0]
0107 if [#<correction_z> GE 0]
0106 repeat [#<repeat_all>]
#<counter>=0
#<counter_x>=0
37 g4 p#<wait_all>
G90 (absolute mode)
G40 (toolradius correction off)
G21
g54 g0 x-20 y[#<correction_y>]
42 g54 g0 z2
0105 repeat [#<repeat_clean>]
s1m3
g4 p#<wait_trigger>
s1m5
47 g4 p#<wait_clean>
0105 endrepeat
g54 g0 x[#<correction_x>] y[#<correction_y>] z[#<correction_z>]
0100 repeat [#<lines>]
0101 repeat [#<squares_per_line>]
52 g90 x[#<counter_x>*#<dist_squares_x>+#<correction_x>]
g90 z[#<correction_z>]
0102 repeat [#<repeat_count>]
0103 repeat [#<square_length>]
```

```

g90 y[#<counter>*#<dist_squares_y>+#<correction_y>]
57 0104 repeat [#<square_length>]
    sim3
    g4 p#<wait_trigger>
    sim5
    g4 p#<wait_pass>
62 g91 G1 y#<spot_distance> f#<move_speed>
    0104 endrepeat
    g91 x#<spot_distance>
    0103 endrepeat
    0102 endrepeat
67 #<counter>=[#<counter>+1]
    0101 endrepeat
    #<counter>=0
    #<counter_x>=[#<counter_x>+1]
    0100 endrepeat
72 (g28)
    (g91 z-22)
    (g91 g1 x6 f100)
    (f#<move_speed>)
    g90 x0 y0 z35
77 0106 endrepeat
    0107 else
        (MSG, You would have crashed! Do not set correction z lower than 0!)
    0107 endif
    0108 else
82 (MSG, You would have crashed! Do not set correction x lower than 0!)
    0108 endif
    0109 else
        (MSG, You would have crashed! Do not set correction y lower than 0!)
    0109 endif
87 %

```

9.2 Profile measurement file conversion (python)

```

import pandas as pd
import matplotlib.pyplot as plt
3 %matplotlib qt

filename="PS_02_layer_1x.csv"

with open (filename, 'r') as f:
8     s = f.read()

with open ('out.txt', 'w') as f:
    for l in s.split('\n') [:23]:
        print(l, file=f)
13     for l in s.split('\n') [24:]:
        print(l[:3] + l[3:].replace(',',';',1), file=f)

df = pd.read_csv('out.txt', encoding="latin1", header=19, index_col=False, sep=";")
18 df.to_csv(filename[:-4]+"_processed1.csv", decimal=",", sep=";")

```